Studies on Orphan Genes in the Newt Limb Blastema

A Dissertation Submitted to
The Graduate School of Life and Environmental Sciences,
the University of Tsukuba
in Partial Fulfillment of the Requirements
for the Degree of Doctor of Philosophy in Science
(Ph.D. Program in Biological Sciences)

ROMAN MARTIN CASCO ROBLES

Table of Contents

1. Abstract

Newts are urodele amphibians that have an outstanding capacity to regenerate various tissues throughout their life, even at their adult terrestrial-life stages. They can regenerate tails, the retina and lens, brain tissues, heart tissues, limbs, and even jaws. They can also regenerate limbs via the formation of a blastema: a mass of progenitor-like cells that accumulates at the site of injury. The exact molecular mechanisms involved in triggering the regenerative response, and blastema formation still remains largely unknown. Previous studies have shown that newts contain similar sets of genes with other organisms including mammals, yet these commonalities in genetics is insufficient to elucidate the reasons why newts can restore missing tissues while other organisms cannot. Recent studies performing *de novo* transcriptome and genomic assembly for *Ambystoma mexicanum*, and *Pleurodeles waltl*, have shown unknown/uncharacterized transcripts are present *in-silico*, however no current study has yet to examine the potential for these transcript's implications during regeneration. Focusing on identifying novel transcripts that may have possible functions during the early process of limb regeneration, this study identified an orphan gene named *Newtic1*, whose transcripts were upregulated in blastema tissue, and whose immune-histochemical expression was found to be present in a subset of erythrocytes. Immunostaining also showed that these *Newtic1* positive cells could form a novel clump called EryCs. These EryCs can form a complex with monocytes and circulate throughout the body. During early limb regeneration, EryCs were detected to form at the distal stump without showing any signs of monocyte interaction, and would also accumulate at the distal blastema as it further developed. Further results also suggest that newt erythrocytes also can express secretory molecules including growth factors and matrix

metalloproteases, and are capable of delivering these molecules into the blastema. Interestingly, when newt adult blastemas were compared with larval blastemas, EryCs were shown to be absent in larval samples, despite having *Newtic1+* erythrocytes in the intact limb region. Taken together, this study demonstrated the capacity for identifying novel genes from *in-silico* analysis, leading to the discovery of the orphan gene *Newtic1,* which was detected in newt tissues. *Newtic1* also led to the identification of novel behavior on erythrocytes which may play key roles in the early regenerative process of the limb. This study can also provide comparative insight as to why other tetrapods, including humans may have restricted regenerative potential. This study can be a milestone for further understanding the roles of erythrocytes within vertebrate physiology other than oxygen transport, and serve as a new starting point toward the elucidation of understanding newt limb regeneration.

2. Abbreviations

AEC	Apical Epithelial Cap
Anti-RFP	Anti- Red Fluorescent Protein
B	Blastema
BMP	Bone Morphogenic Protein
Bp	Basophilic Normoblasts
DPA	Days Post Amputation
EB	Early Bud Blastema
ED/MD/LD	Early Digits/ Medium Digits/ Late Digits
EDD	Early De-Differentiation
EF1α	Elongation Factor 1 alpha
EryCs	Erythrocyte Clumps
IS-Transcripts	In silico transcripts
JNRC	Japan Newt Research Community
LB	Late Bud Blastema
LDD	Late De-Differentiation
MB	Medium Bud Blastema
MEB	Moderate Early Bud Blastema
MMPs	Matrix Metalloprotease
NL	Normal Limb
OcNobs	Orthochromatic Normoblasts
Pal	Palette stage
PcNobs	Polychromatic Normoblasts
Prod1	Proximal Distal 1
SRA	Sequence Read Archive
TGFb-1	Transforming Growth Factor beta 1
Vim	Vimentin
WE	Wound Epithelium
WH	Wound Healing

3. Introduction

3.1 The Japanese-Fired Bellied Newt as a Model for Regenerative Studies

The newt, *Cynops pyrrhogaster,* is a urodele amphibian that displays an incredible ability to regenerate various body parts and tissues such as the limbs, tail, cardiac tissues, nerve tissue, retina and lens (Fig. 1). This animal is the only known tetrapod that can regenerate this array of tissues even at the terrestrial-life stage; in other words, as adults. Their ability to regenerate is executed mainly through complex mechanisms of trans-differentiation, reprogramming and/or dedifferentiation of cells, as in the case of limb regeneration; producing a mass of progenitor-like cells which ultimately restore the missing body part. This mass of cells is also known as the *blastema* (Avarado et al, 2008; Eguchi et al, 2011; Simon and Tanaka, 2013; Islam et al, 2014; Tanaka et al, 2016, Casco-Robles et al, 2016). Although salamander regeneration has been extensively studied for more than 200 years, beginning with Spallanzani's observations in his book "the Prodromo" around in the late 1700's (Tsonis and Fox, 2009), the molecular/cellular mechanisms that are involved in these processes remain largely unknown. Among this group of urodeles; the species that have had much academic spotlight are the eastern newt *Notophthalmus viridescens*, the Japanese-fired bellied newt, *Cynops pyrrhogaster*, the Iberian-ribbed newt, *Pleurodeles waltl*, and the mexican axolotl, *Ambystoma mexicanum*, with the overall aim to unlock the mystery of this regenerative power. Having this in mind, the focus of this study is to elucidate the early process of limb regeneration with *C. pyrrhogaster*.

Generally, regeneration is defined as the ability to restore lost body parts, either self-induced, simple restoration of degrading tissues/ cells, or as a result from traumatic injury. Many invertebrates such as the planarian, sponges, hydras, or starfish, have an extremely high regenerative ability, but their body structure and physiology are much different from ours, and the

function of their regeneration would ultimately be reproduction, and budding of new body parts via neoblast (Tanaka and Reddien, 2011; Looso, 2014). Regarding vertebrates, teleost fish can regenerate their fins, larval anurans can regenerate limbs, even mammals such as mice and humans can regenerate the distal finger tips but are severely limited at more proximal tissue (Brockes and Kumar 2008; Nacu and Tanaka, 2011; Stocum and Cameron 2011). On the other hand, urodeles are the only tetrapod vertebrates that can regenerate limbs as well as other tissues throughout their life cycle. The newt is closely related to us from an evolutionary standpoint, and the function of regeneration is to save its life independently of reproduction, in other words, regeneration should occur even when the organism has sexually matured, passed the limit of bearing eggs, and producing offspring. Therefore, studying regeneration in the newt can provide insights in regenerative medicine on how to treat patients with traumatic damage to various body parts or that have had a sickness that has resulted in a loss of organs or tissues, or even age-related degenerative diseases (Godwin, 2014; Al-Qattan et al., 2014; McCusker and Gardiner, 2014).

3.2 Limb Regeneration

Extensive research has accumulated regarding the mechanics of limb regeneration of salamanders (Stocum and Cameron, 2011; Tornini and Poss, 2014; Iten and Bryant, 1973; Simon and Tanaka, 2012). The overall process of limb regeneration can be seen in Fig. 2 (modified from Iten and Bryant, 1973). Upon amputation of the limb, the wound is sealed by a blood clot triggered by thrombin. Epidermal cells from the edge of the injury lose their intercellular junctions (Hay and Fischmann, 1961), and migrate to the wound site developing a layer called the wound epithelium (WE) (Brockes and Kumar, 2002). Following the formation of the WE, histolysis commences on various tissues in the proximity to the wound site. The extracellular matrix begins to degrade as proteolytic enzymes, such as lysosomal acid hydrolases and matrix metalloproteinases (MMPs)

begin to surge (Dresden et al 1970, Ju et al, 1998, Gardiner et al, 1999, Imokawa et al, 1996). MMPs also prevent reassembly of a basement membrane, giving more opportunity for contact between the WE and the underlying tissue (Godwin et al. 2013). As histolysis has progressed, there is a change in transcriptional profiling. Cells from the underlying tissue begin to lose their differentiated phenotype, and also begin to express genes to those in: limb development of the embryo, cell stemness, reduction of cell stress, and remodeling internal structure (Gardiner et al 2002, Geraudie et al. 1998, Rao et al. 2009). Afterwards, the WE becomes innervated with regenerating nerves from the stump (Singer, 1974). The WE thickens into the Apical Epithelial Cap (AEC), and serves as a signaling center secreting fibroblast growth factors and morphogens, that serve as chemo-attractants and mitogens, to begin the formation and expansion of the blastema (Endo et al., 2004; Mullen et al., 1996). Connective tissue cells then migrate from various locations and provide cues as to their position. Cells having different positional identity interact, and begin to proliferate, and cells having intermediate position are generated until the patterning of the missing structure is complete. As the blastema cells differentiate into their corresponding tissues via positional identity, the new tissues effortlessly integrate with the old limb structures, and the missing structure is re-established (Bryant et al., 1981; McCusker and Gardiner, 2014; Monaghan et al., 2012).

3.3 Prod1 - A Salamander Specific Protein

It has been a long sought issue whether such exceptional ability of the newt can be explained by genes conserved in vertebrates including humans or by unique genes that the newt may have evolved (Kumar et al, 2007; Looso et al, 2013). Recognizing that the newt has an exceptional regenerative ability unavoidably leads to the following questions: Why can this small

amphibian perform such a staggering action, while other organisms cannot, and moreover, how is it able to do so (Garza-Gracia et al., 2010)? Scientists believe that the newt must contain and rely some key genetic mechanisms that might be conserved in the genome of other organisms (Simon and Tanaka, 2012) but may lay static or require other mechanisms. Understanding the newt's genome is fundamental to unlocking this ability (Gardiner et al., 2002). From an evolutionary perspective, salamanders are much older than higher, more recent organisms down the evolutionary tree; therefore it may be plausible that a conserved mechanism would be hidden within our own genome. In contrast, some regard this regenerative ability to have evolved locally among salamander species having specific molecules or mechanisms that are not known (Garza-Gracia et al., 2010). da Silva et al. 2002, was able to identify a newt ortholog of CD59, called *Prod1*, which is three finger cell-surface protein having a GPI-anchor, and was shown to be implicated in the local cell-cell interactions regulating positional identity (da Silva et al., 2002). The ligand to *Prod1* was found to be newt anterior-gradient protein (nAG), where their protein-protein interaction regulates patterning and growth. This interaction makeas the positional identity of cells possible, and therefore is essential to the regenerative process (Kumar et al., 2007). *Prod1* was also found to be specific to be conserved in salamander amphibians only (Garza-Gracia et al., 2009, 2010). This discovery can give insight that the regenerative capacity of salamanders might have evolved locally and not related to a conserved mechanism as previously thought, and that they possess unique genes which influence this overall process.

3.4 Salamander Transcriptomics

Despite significant knowledge accumulated over the years with respect to cellular reprogramming, signaling pathways, and proximal distal patterning, involved in the newt regeneration (Stocum and Cameron, 2011; Tanaka and Reddien, 2011), many studies have been

hindered by a scarce amount of genomic data found in public databases. This is due to the massive size of the newt's genome and the lack of a reference genome, and limited amount of tools and techniques needed to analyze genetics of this organism (Poss K., 2010, Alvarado et al., 2006). However, in the past years recent transgenic protocols have been established which has enabled studying the functions of genes that may be crucial for regeneration (Tsonis et al., 2011; Casco-Robles et al., 2011).

In the past decade, high throughput next generation sequencing technologies (NGS) have emerged to provide faster sequencing of large amount of data in a relatively short period, while at the same time having dramatic price cuts. This enables laboratories to reconstruct transcriptomes from RNA-seq data even from those organisms that do not have a reference transcriptome at their disposal, by means of *de novo* assembly (Grabherr et al., 2010). Several laboratories assembled *de novo* transcriptomes emphasizing on the regenerative ability of salamanders, such as *Notophthalmus* transcriptome (Igor et al, 2013) and the more recent *P. waltl* transcriptome, which also created a 20Gb genome emphasizing on the expansion of embryonic stem cell-specific miRNA, and harbinger DNA expanded throughout the genome, and co-expressed during limb regeneration (Elewa et al, 2017). Going a step further, a recent study on the axolotl, also developed a massive 32 Gb genome, provides evidence that intron size in developmental genes is under constraint and that species-restricted genes may contribute to limb regeneration (Nowoshilow et. Al, 2018). A study conducted by Looso et al. (2013), which established a *de novo* transcriptome of regenerating tissues including the heart, limbs, and eye, had identified 826 proteins that were specific to Urodele amphibians. This same year, Abdullayev et al. (2013), working also with *Notophthalmus,* was able to annotate 19,903 newt proteins. Researchers working with the axolotl also have established *de novo* transcriptomes, identifying *in silico* transcripts belonging to the

salamander group (Wu et al., 2013; Stewart et al., 2013). An axolotl study, comparing wound healing stage and amputated limbs, found 93 amputation-associated genes (Knapp et al., 2013). More recently, a *Cynops* transcriptome of the regenerating eyeball was constructed, obtaining 237,120 transcripts, in which 17,316 protein coding transcripts can possibly be unique to the newt (Nakamura et al., 2014).

3.5 Development of the *C. pyrrhogaster* Transcriptome

To understand the regenerative capacity of the newt, it is fundamental to obtain genomic or transcriptomic data regarding the expression of particular genes at specific times, and at particular tissues/organs. The Regenerative Physiology Laboratory of Dr. Chikafumi Chiba, being a major contributor for the Japan Newt Research Community (JNRC), embarked on establishing a comprehensive *de novo* transcriptome by the collaboration of multiple universities and investigators across Japan. In contrast to other newt species, *C. pyrrhogaster* has been studied across a broad spectrum of life science fields such as gametogenesis, reproduction, fertilization, embryogenesis, metamorphosis, regeneration, chemical sense and behavior, toxicology, evolution, and ecology/preservation (Eto et al, 2009; Yokoe et al, 2014; Yokoe et al, 2016; Kon et al, 2017; Ueno et al, 2014; Mutua et al, 2014; Takano et al, 2011; Yanagi et al, 2015; Chiba et al, 2012; Sousounis et al, 2015; Inoue et al, 2010; Iwata, et al 2013; Nakada et al, 2014; Nakada et al 2017; Kudo et al 2017; Tominaga, et al, 2013; Tominaga et al, 2015; Tominaga et al 2016; Tominaga 2018), so creating transcriptomes from various tissues such as the regenerating eye, regenerating heart, regenerating brain, blastema, visceral organs (lungs, small intestines, liver, pancreas, and kidneys), intact limb, embryo, testes, ovaries and oviduct, olfactory epithelium, and vomero-nasal organ would be of invaluable use to elucidating more processes and mechanisms this animal executes. mRNA-seq was performed by Illumina-Hi Seq platform, and these transcriptomes were

assembled using Trinity tool (version 2012-10-05). Aside from establishing individual tissue transcriptomes, all the filtered reads (2,177,126,832 reads), from each transcriptome were bundled together, removed bacterial sequences, and re-assembled into a comprehensive TOTAL transcriptome resulting 697,670 transcripts. The present study contributed to the intact limb and blastema transcriptome. Assemblies can be found at http://antler.is.utsunomiya-u.ac.jp/imori/, which displays sequence read archive (SRA) ID from NCBI repository site displaying corresponding contributors. The website, http://antler.is.utsunomiya-u.ac.jp/~fubito/database/imori/ (Nakamura et al, 2014), can provide BLAST result data and annotation of individual transcriptomes (Fig. 3).

3.6 Purpose and Goal of This Study

To address the question as to why newts can carry out regeneration exceptionally, I hypothesized that the newt must have proprietary genes involved in the process of limb regeneration. The purpose of this study is to screen for novel genes that are specific to the newt and involved in the regenerative process via *in silico* transcriptome analysis. Despite the rapid onset of transcriptomes that have been constructed for salamander species in and screen for salamander specific and unique transcripts have been obtained, these transcripts have only been analyzed at most by real time-PCR and protein mass spectrometry. There has yet to be a study that focuses primarily on these unique sequences, and functionally annotates them. The defining goal of this study is to perform a functional analysis of screened novel genes by the use of a conditional knockdown system using Cre/loxP recombinase, and decreasing the expression of these novel genes with the use of shRNA (Casco-Robles et al., 2011). The CRISPR/Cas9 system could also be applied to completely knockout these genes to analyze their function (Fig. 4).

4. Materials and Methods

4.1 Animals and Surgical Procedures.

Adult and larval Japanese fired bellied newts, *Cynops pyrrhogaster*, were used in all experiments performed in this study. Larval and adult (total body length: male, ~9 cm; female, 11–12 cm) Toride-Imori were used for the construction of transcriptome databases, molecular cloning, and examination of larval blood and limbs. Adult newts that were captured from Okayama, Kyoto, Fukushima and Miyagi Prefecture by a supplier (Aqua Grace, Yokohama, Japan) were also used for the examination of adult blood and limbs. Adults were kept at 18^{o}C, under natural light conditions, and reared in large polyethylene containers, filled up to 15cm of water. The containers would slightly be elevated from one end to enable a dry area, and a water area for the newts. Water would be renewed twice daily. Newts were given frozen blood worms as a dietary source (Nakamura et al, 2014; Chiba et al., 2012). Each box would contain approximately 80-150 newts, independent of gender, or size. Larval newts were reared in plastic ice-cream cups holding 50ml of distilled water, which would be renewed daily. They were fed brine shrimp as a dietary source, until they are large enough to eat frozen blood worms (Nakamura et al, 2014).

For surgical procedures, animals were kept at 22^{o}C, contained within small plastic containers having 2 sheets of damp paper towels. Before any surgical procedure, animals were anaesthetized with 0.1% FA-100 (4-allyl-2-methoxylphenol, DS Pharma Animal Health, Osaka, Japan) diluted in distilled water at room temperature (RT:22^{o}C) for 1hr and 45min (larval newts were left for 30min). After sedation, adult newts were rinsed in distilled water and lightly dried on paper towels. Larval newts were rinsed in distilled water. All newts were amputated at the right forelimb mid-zeugopodial region under a dissecting microscope (M165 FC; Leica Microsystems, Wetzlar, Germany), using a blade: for larvae, tip of the blade (Cat#: 4991482; Feather Safety

Razor, Osaka, Japan); for adults, a surgical blade (No. 14; Futaba, Tokyo, Japan)) (Tanaka et al, 2016; Nakamura et al, 2014). Animals were then left to recover and regenerate in the same rearing conditions, until the desired regenerating stage was collected. A second amputation was then performed at the mid stylopodial region to collect the regenerate sample, which was then fixed in Zambonis solution for 6h at 4^{o}C for immunostaining procedures. For samples used in RNA isolation or western blotting, the second amputation was quickly done 1mm proximal to the first amputation site in the case of intact limb tissue, or at the base of the blastema. The regenerative stages were collected as follows: adult tissues were collected at 0DPA (amp), 5 DPA (stage I – WH/EDD), 14 DPA (Early Stage II – LDD/MEB/EB), and 27 DPA (Stage III - MB). Larval limb stages were collected at 0 DPA stage and the Stage III. For adult splenic tissue collection, an incision was made at the anterior midsagittal plane beginning from the mid thoracic towards the lower abdominal quadrant. The spleen was collected from the animals, and quickly placed into Zambonis solution for immunostaining (Tanaka et al, 2016; Nakamura et al, 2014).

4.2 PCR and Molecular Cloning

Total RNA of limb tissues and adult blood was extracted using TOTAL RNA Isolation Nucleospin kit II (740955.50, MACHEREY-NAGEL GmbH & Co. KG, Duren, Germany) using the manufacturer's instructions. Three independent specimen samples were used per RNA collection, and cDNA was synthesized using Superscript II Reverse transcriptase kit (18064-014, Invitrogen in Thermo Fisher Scientific, Tokyo, Japan) with oligo(dT) 12-18 primers (18418012, Invitrogen in Thermo Fisher Scientific). Parameters were configured according to the manufacturer's instructions. In the case of limb tissues, blastema samples were weighed, and the equivalent mass for intact tissue was also collected. RNA was then extracted. Same RNA

concentration of blastema and intact limb samples were used synthesize cDNA, and stored at -20°C. Genomic DNA was collected using approximately 200µl of heart blood using the Wizard Genomic – DNA Purification Kit (Cat. # A1120, Promega; WI, USA), and stored at 4°C. Concentration of samples was measured using Nanodrop-1000 (Nanodrop ND-1000 Spectrophotometer, Thermo-Fisher Scientific, Wilmington, Delaware, USA). Molecular cloning was performed using cDNA, or genomic DNA of these tissues, with either KODFX kit (KFX-101, Toyobo, Tokyo, Japan) or Adv. II PCR kit (Cat. 639206,Takara Bio, USA), while applying standard PCR conditions using a MJ Mini Gradient Thermal Cycler (PTC-1148, Bio-Rad, Hercules, CA, USA). All primer sets were ordered from www.eurofinsgenomics.jp, and can be found on Table 2, showing primer sequence, annealing temperature, and cycle number. Primers were made from the *de-novo* assembled TOTAL transcriptome on IMORI website (http://antler.is.utsunomiya-u.ac.jp/imori/). Sanger sequencing was performed as previously described (Tanaka et al, 2016; Nakamura et al, 2014) using standard sequencing protocols. PCR products were subcloned into *Escherichia coli* using a TA cloning system (45-0640, TOPO TA Cloning Kit, Dual Promoter; Thermo Fisher Scientific) and then sequenced by Sanger protocols (ABI 3130; Applied Biosystems, in Thermo Fisher Scientific).

4.3 RNA High Throughput Sequencing.

All tissue RNA samples needed to be sequenced were sent to Hokkaido System Science Inc. (Hokkaido, Japan) for RNA-sequencing using Illumina HiSeq-2000 Pair-end 100. RNA integrity (having RIN > 8.0) was evaluated using Agilent Bioanalyzer. Read data were cleaned and filtered by removing adaptor sequences using cutadapt command-line tool (https://code.google.com/p/cutadapt/). Any reads containing "N" nucleotides were also removed.

Cleaned reads were then assembled into contigs via the TRINITY assembler tool (version 2012-10-05; Grabherr et al., 2010) https://github.com/trinityrnaseq/trinityrnaseq/wiki; applying preset parameters.

4.4 In-silico isolation of Newtic1 Contig.

Newtic1 sequence was obtained by subtracting *C. pyrrhogaster* intact limb components from blastema transcriptome via blastn ncbiblast-2.2.28+ applying default parameters along with a e-value of $E \leq 0.001$ (ftp://ftp.ncbi.nlm.nih.gov/blast/executables/blast+/2.2.28/). Intact limb tissue transcriptome was set as a database and the blastema transcriptome as a query. Those blastema contigs having no alignments were separated using "NO-HIT" parsing script, and short transcripts (< 950bp) were removed. Remaining transcripts were then subjected to blastx, against non-redundant (NR) NCBI database via BLAST2GO software (Conesa et al, 2005) for annotation and mapping. Those contigs that had no annotation were further aligned with the EYE transcriptome. Matching contigs were collected, and subjected to protein prediction using EST scan (https://myhits.isb-sib.ch/cgi-bin/estscan), and those with no prediction/short peptide sequence were disregarded. Remaining peptide sequences were compared to TOTAL transcriptome database, and the longest contig equivalents were collected. Finally, these sequences were subjected to BLAST2GO again for annotation, subject to NR annotation and Interpro-Scan domain analysis (https://www.ebi.ac.uk/interpro/search/sequence-search), and those sequences that are either known genes, had no predicted domains or not found in other newts were removed.

4.5 Tissue Section Preparation

For immunolabeling, larval and adult tissues were fixed in modified Zamboni's fixative (2% paraformaldehyde (PFA)/0.2% picric acid in phosphate-buffered saline (PBS; pH 7.5)) at 4 °C for 6h. In larval tissue staining and blood smear experiments, tissues were fixed in 4% PFA in PBS (pH 7.5) at RT for 2 h. Fixed tissues were washed thoroughly with PBS at 4 °C (15 min × 3, 30 min × 3, 1 h, and 6 h), and then allowed to equilibrate in 30% sucrose in PBS at 4 °C. The tissues were embedded in Tissue-Tek, O.C.T. Compound (4583; Sakura, Finetek USA, Inc., Torrance, CA, USA), frozen at about −30 °C in a cryotome (CM1860; Leica), sectioned at about 20 μm thickness, attached on gelatin-coated cover slips, and then dried at RT for a few hours. The sections were stored at −20 °C until use.

4.6 Blood Cell Collection, Preparation, and Smear Staining.

Peripheral blood was collected from forelimbs immediately after amputation. For the Wright-Giemsa stain, and the α-naphthyl acetate esterase stain, blood was spread on a glass slide to prepare the blood smear and air dried. For the former stain, the blood on the slide was fixed in 100% methanol for 30 min and air dried. For the esterase stain, the blood on the slide was fixed in citrate acetone formaldehyde solution (SLBQ6227V; Sigma-Aldrich in Merck, Tokyo, Japan) for 30 sec at RT, and then rinsed thoroughly in running deionized water (DW) for 45–60 sec. These samples were immediately processed for staining (see below). For immunolabeling (Fig. 12a,b), blood was added directly to 4% PFA fixative in a glass bottom dish (D112310; Mastunami, Tokyo, Japan) and then incubated at RT for 2 h. In some experiments, blood was fixed in modified Zamboni's solution at RT for 2 h. Fixed blood cells in suspension were carefully washed with PBS at 4 °C (20 min × 3) and immediately used for labeling. Blood cell suspensions were gently stirred

periodically during incubation to prevent coagulation, and solutions were carefully exchanged by micropipettes under a dissecting microscope so as not to lose or select cells. In experiments to examine EryC-monocyte complexes, blood was put on the bottom of the dish and allowed to coagulate for a few minutes, and then fixed in modified Zamboni's solution at 4 °C for 6 h. The coagulated blood was carefully washed with PBS at 4 °C (20 min × 3) and immediately used for labeling.

To characterize blood cells in the adult newt, each blood smear was stained using a standard Wright-Giemsa system (15021; Muto Pure Chemical Co., Ltd, Tokyo, Japan) according to the manufacturer's instructions. Cell types were identified according to established criteria (Claver et al. 2009, Giger et al. 1930, Pfeiffer et al. 1990) . Monocytes were further characterized using a α-naphthyl acetate esterase staining system (SLBQ6227V; Sigma-Aldrich in Merck) according to the manufacturer's instructions. Immunolabeling of blood cell suspensions was carried out as for tissue sections (see below).

4.7 Antibodies

The following primary antibodies were used: anti-rabbit anti-Newtic1 synthesized by Sigma-Aldrich using amino acid sequence in Fig. 7 (1:200;Sigma-Aldrich), anti-mouse anti-vimentin (1:500;ab28028;Abcam,Tokyo 103-0012, Japan), anti-rabbit anti-RFP (1:500;,600-401-379, Rockland Immunochemicals, PA 19468, USA), anti-rabbit anti- TGFβ-1 (1:500; CYT4632, celltechgen, LLC TX 77079,USA), and anti-rabbit anti-BMP2 (1:500; LS-B13128; Lifespan BioSciences). Secondary antibodies were as follows: Alexa Fluor 488-conjugated goat anti-mouse IgG (H + L) (1:500;A11001: Thermo Fisher Scientific), Rhodamine (TRITC) – conjugate affiniPure goat anti-rabbit (1:500; Code: 111-025-003; Jackson ImmunoResearch Laboratories,

West Grove, PA 19390, USA), Biotinylated anti-rabbit IgG (1:500; Vector laboratories BA-1000) . Nuclear stains used were 4,6-diamidino-2-phenylindole; DAPI (1:50,000; D1306; Thermo Fisher Scientific), TO-PRO-3 Iodide (1:50,000; T3605; Thermo Fisher Scientific), or Mayer's haematoxylin solution (131-09665; Wako Pure Chemical Industries, Ltd., Osaka, Japan). Antibodies are summarized in Table 4.

4.8 Immunohistochemistry.

The same procedures for single or double immunofluorescence labeling were applied to both tissue sections and blood cell suspensions. For single labeling with a certain primary antibody or double labeling with two primary antibodies produced in different species, the following protocol was applied: samples were washed thoroughly (PBS, 0.2% TritonX-100 in 1x PBS, PBS; 15 min each), incubated in blocking solution (5% bovine serum albumin (BSA, 050 M 1599; Sigma-Aldrich in Merck)/2% normal goat serum (S-1000; Vector Laboratories, Burlingame, CA, USA)/0.2% TritonX-100 in PBS) for 2 h, washed as before, and then incubated in primary antibody (antibodies) diluted with blocking solution at 4 °C for 15 h; after washing thoroughly, the samples were incubated in secondary antibody (antibodies) diluted with blocking solution for 4 h and washed thoroughly. For double labeling with two primary antibodies produced in the same species, entire labeling procedures mentioned above were repeated serially. In the case of double labeling of TGFβ-1 and Newtic1, or BMP2 and Newtic1, samples were labeled with primary antibody to TGFβ-1 or BMP2 and alexa-488 conjugated secondary antibody. Subsequently, the same samples were labeled with Newtic1 primary antibody and rhodamine-conjugated secondary antibody. In the case of blood cell suspensions, samples at the bottom of the dish were gently stirred, and solutions were carefully exchanged as for sample preparation. In any labeling protocol, after

samples were stained and washed, the nuclei of cells were counterstained with either Mayer's hematoxylin, DAPI, or TO-PRO-3 Iodide. Tissue sections were finally mounted on a glass slide with 90% glycerol in PBS or into VECTASHIELD mounting medium (H-1000; Vector Laboratories). Tissue sections and blood cell suspensions were immediately subjected to microscopic analysis.

4.9 Western Blotting

Protein samples were prepared from red blood cells or limb tissues (blastema tissue mass was weighed and the equivalent 0 DPA tissue mass was harvested) were collected in lysis buffer solution (Tris 25mM, NaCl 150mM, EDTA*2Na 1mM, 1% Igepal CA-630, 1% Sodium deoxycholate, 0.1% SDS) having 1% proteinase inhibitor cocktail (P8340,Sigma-Aldrich). Samples were subjected to protein extraction using standard procedures. Proteins were separated by loading 20µl in 10% Gelcast wells (#456-1033, Mini-PROTEAN TGX Precast Gel, Bio-Rad, Hercules, CA, USA) by SDS-PAGE, and western blotting was performed as previously described (Susaki and Chiba, 2007; Mizuno et al., 2012; Yoshikawa et al., 2012). In brief, after separation with Gelcast, proteins were transferred to an immune-blot PVDF membrane (Cat. 1620-174, Bio-Rad labs Inc., USA). Membranes were washed in TBST for 10min, then incubated for 1h in blocking solution (3% BSA, 1% TBST, and 2% AvidinD; Avidin/Biotin Blocking kit, SP-2001, Vector Laboratories). Afterwards, the membrane was rinsed for 1min, 10min, then for 20min, and then incubated in primary antibody diluted in blocking solution (3% BSA, 2% biotin; Avidin/Biotin Blocking kit, and anti-rabbit anti-Newtic1 antibody; 1:200) at 4^{o}C, overnight. After incubation, membrane was washed in TBST (1min, 15min x 3), and then incubated with secondary antibody (3% BSA, 1% TBST, and biotinylated anti-rabbit IgG, 1:500) for 90 min at RT. Washing

step was repeated, and samples were incubated in Avidin Biotin Complex solution (1% TBST, 2% Avidin, and 2% Biotin; Vectastain ABC Elite kit, PK-6100, Vector Laboratories) for 90 min at RT. Washing was repeated, and the sample was then subjected to DAB staining kit (DAB substrate kit, SK-4100; Vector Laboratories). After adequate coloration, membranes were washed in chilled distilled water for 5min x 6. Membranes were then scanned and analyzed.

4.10 Red Blood Cells Purification.

Blood was collected directly from adult newt hearts using a 23G x 1¼" needle (NN-2332S, Terumo) with a 1ml syringe (130803F, Terumo). Approximately 100µl of PBS was first drawn into the syringe. The needle was inserted at a 45^{o} angle just above the clavicle into the heart. Between 130µl - 200µl of blood was slowly extracted from the animals. Blood samples were immediately loaded onto pluristrainers of 15µm mesh (43-50015-01, Pluriselect, Germany) to retain red blood cells but remove smaller cells. Strainer was lightly shaken 5 min x 3, and blood cells were gently pipetted every 10min. Procedure was repeated three times. Afterwards, 3 ml of filtered blood was gently pipetted into a 15 ml centrifuge tube, containing 3 ml of Ficoll solution (30% Ficoll in PBS), without mixing. Samples were then centrifuged at 100G for 20 min, using a TOMY LC-120 basket centrifuge (LC-120, Tomy Seiko Co., LTD., Japan). Red blood cell pellets were carefully extracted (aprox. 120µl), and a small quantity (approximately 5 µl) was observed for purity under the microscope. The remaining pellet was used for the RNA isolation procedure.

4.11 Gene Expression Profiling of Blood Cells

Total RNA was purified from whole blood samples (n = 3) and mRNA-seq was carried out in a manner similar to the construction of transcriptome databases (see above). To investigate the relative expression levels of genes, sequence reads (deposited to NCBI, SRP034152, SAMN08574272-08574274) were aligned along *IS*-transcript sequences from TOTAL transcriptome using the trinity script align_and_estimate_abundance.pl (–est_method RSEM;–aln_method bowtie2). Subsequently, from 168,047 mapped IS-transcripts, 304 IS-transcripts were manually screened encoding secretory molecules including growth factors and MMPs, and then calculated the mean ± SE of expression levels (normalized FPMK) for each secretory molecule gene. Next, to confirm the expression of these genes in polychromatic normoblasts (PcNobs) by PCR, PcNobs (>99%) were purified from whole blood cells (Fig. 19B). Whole blood cells collected in PBS were loaded, at 130–200 μl each, onto pluristrainers (15 μm mesh, 43-50015-01; Pluriselect, Germany) placed in 100 ml beakers filled with 40 ml PBS. The strainers containing blood cells were gently shaken in PBS for 15 min and then blood cells in the strainers were mixed using 500 μl micropipettes. This procedure was repeated three times. Subsequently, 3 ml of blood cell suspensions was carefully transferred onto 3 ml of ficoll solution (30% Ficoll PM400 (Type 400; Sigma-Aldrich in Merck) in PBS) in 15 ml tubes. The tubes were then centrifuged at 100G for 20 min (LC-120; Tomy Seiko Co., Ltd., Tokyo, Japan). PcNobs deposited on the bottom (about 120 μl) were carefully transferred into a microtube. A small quantity (5 μl) of cell suspension was sampled and recovered in PBS to observe its purity under a microscope. The remaining pellet of PcNobs was used for cDNA synthesis followed by PCR analysis.

4.12 Image Acquisition and Analysis

Bands on agarose gels in PCR and protein bands on membranes in Western blotting were scanned and quantified by NIH ImageJ software (https://imagej.nih.gov/ij/). Transmitted light and fluorescence images of tissue sections and blood cells were acquired either by a charge coupled device (CCD) camera system (DP73; cellSens Standard 1.6; Olympus, Tokyo, Japan) attached to a fluorescence microscope (BX50; Olympus) or through a confocal microscope system (LSM510; LSM 5.0 Image Browser software; Carl Zeiss, Jena, Germany). Microscopic images were analyzed by Photoshop CS5 Extended (Adobe Systems, San Jose, CA, USA) as well as with software for the image acquisition systems. In experiments to quantify the concentrations of growth factors in PcNobs, I selected representative images (for TGFβ-1, six images (total number of PcNobs: 40, 53, 71, 84, 89, 120) from six experiments; for BMP2, three images (total number of PcNobs: 88, 123, 135) from three experiments), that were acquired with a 20× object lens by the BX50-DP73 system. For each image, I measured the amplitude of the mean luminance of the cytoplasm of each PcNob against the background using a function in Photoshop, and normalized the values against the maximum in the same image so that data among experiments could be compared. Figures were prepared using Photoshop.

4.13 Blastema Cell Counting

In blood smear and cell suspensions, the proportion of cells was estimated by counting the number of cells in representative microscopic images (total cell number/view field >50) obtained from at least three independent experiments. The images were acquired with a 20× object lens by the BX50-DP73 system. In tissue sections, representative images were also obtained from at least three independent experiments. Images covering the area to be analyzed were acquired at high

resolution through the confocal microscope system, and merged into one image. In experiments to estimate the proportion of Vimentin positive cells (Vim+ cells) and the number of Newtic1+ clumps in blastema at 5 DPA and 27 DPA, I examined representative tissue sections from four individuals at each DPA. For these tissues, limb samples were sectioned along the dorso-ventral axis and used the sections around the central axis of the limb. Only cells that showed a clear nucleus were counted. For vim+ cells, vimentin-immunoreactive cells with a spherical shape, like monocytes, were counted. For Newtic1+ clumps (i.e., EryCs), clumps composed of at least six Newtic1+ PcNobs were counted.

4.14 Statistics

Data in the text are presented as the mean ± SE. The statistical mean difference was evaluated by a Student's t-test, except when data were not homoscedastic, in which case Welch's t-test was applied, by using Excel-Toukei 2008 software (Social Survey Research Information, Tokyo, Japan)

All relevant cleaned mRNA-seq data have been deposited in NCBI (Sequence Read Archive ID, SRP034152; BioProject ID, PRJNA231688; BioSample ID, SRS515156, SRS589430, SRS685575-685579, SRS685581, SRS685583, SRS685585-685595, SAMN08574272-08574274). The lists of contigs that have been annotated are available in IMORI (http://antler.is.utsunomiya-u.ac.jp/imori/).

5. RESULTS

5.1 In-Silico Screening of Unique Transcripts and Validation of Newtic1

Tissue samples were collected from the normal limb (NL) samples and the blastema (B) for RNA-sequencing (Fig. 5). To identify newt specific sequences that were upregulated within blastema tissues, it was necessary to compare blastema transcriptome (*105,467 in-silico* transcripts) with the intact limb transcriptome (flowchart can be seen on Fig. 6), and remove those sequences that were found in both intact tissue and blastema tissue, and have annotation to public databases. Subtracting the intact limb components from the Blastema contigs led to the following: by applying cutoff e-value < 0.001; 64,020 transcripts having higher e-value were removed, leaving 41,447 transcripts that were specific to the blastema transcriptome. Among these 41K transcripts, those that have short read lengths (cut-off less than 950bp) were also removed, resulting in 1,428 blastema specific transcripts. After being subjected to BLAST2GO annotation, 785 transcripts were removed due to having annotation to online databases, leaving 643 blastema specific NO-HIT transcripts. Verifying whether or not these unknown transcripts may be the result of error/artifacts, they were subsequently compared to the newt eye transcriptome. Common sequences were identified in 521 transcripts between both transcriptomes, and remaining sequences were removed. Protein prediction of these 521 transcripts revealed that only 72 sequences had *in-silico* potential prediction for peptide sequences (cut-off amino acid length $\geq$ 100 a.a.). Finally, after comparing the 72 sequences with the TOTAL transcriptome to harvest the longest contig length equivalents, and re-blasting to NCBI databases for further filtering, only 2 complement sequences remained to be unknown, present in blastema, common to other transcriptomes, and having potential for peptide translation. This sequence was called ***Newtic1:*** contig ID: Comp507633_c0_seq1 (3,017 bases) (Fig. 7A), and Comp507633_c0_seq2 (3,006

bases) reverse complement, collected from the TOTAL transcriptome. Its predicted peptide sequence consisted of 375 amino acids (Fig. 7B). Primer sets indicated by a black underline were used to amplify the cDNA/genomic DNA, and used for Sanger sequencing. Interestingly, genomic DNA Sanger sequencing revealed that there are no introns within the gene sequence. Theoretical domains (Fig. 7C) consists on a non-cytoplasmic domain, transmembrane domain, and a cytoplasmic domain. Interestingly, performing a comparative alignment with *N. viridescens* (Igor et al, 2013), *P. waltl* (Elewa et al, 2017), and *A. mexicanum* (Nowoshilow et. Al, 2018) transcriptomes show that Newtic1 protein is conserved among all species with slight variations (Fig. 8A). Developing a phylogenetic analysis shows the relationship between the 4 urodele species using a neighbor-joining method (Fig. 8B). This shows that *C. pyrrhogaster* has a more stringent evolutionary link toward *N. viridescens*, and *P. waltl*, in their regenerative potential, as opposed to the axolotl, which does tend to lose some regenerative ability as adults, or after induced metamorphosis (Monaghan et al. 2014, Weisrock et al. 2006).

5.2 Validation of Newtic1

After obtaining the coding sequence of Newtic1 from Expasy translator (https://web.expasy.org/translate/), primers sets were developed to clone Newtic1's coding region and UTR. Using stage III (27DPA – MB) blastema cDNA as a template, PCR analysis revealed bands at the desired target sites as can be seen in Fig. 9A. Samples of genomic DNA from newt blood were also collected, purified, and tested to verify if Newtic1 was also present in genomic samples. PCR bands at the 1,512bp and at the 76bp display target bands for using two different primer sets (Fig. 9A). Sanger sequencing data showed that both genomic DNA and cDNA samples contained the same amplicon size (Fig. 7A). This also indicates that genomic DNA shows no

apparent introns. Performing a semi-quantitative analysis of PCR (measuring the various PCR band intensity by Image J software), by comparing normal limb (NL) and blastema (B) cDNA, Newtic1 expression reveals higher expression levels in the blastema when normalized with EF1α (Fig. 9B)(n=6). It is important to note that in some trials, Newtic1 was showing a dim band in general, indicating low expression in the overall samples. Using a custom antibody ordered from Sigma-Aldrich constructing a specific epitope, Western blot assay showed that anti-Newtic1 antibody was able to detect a protein band at the predicted molecular weight of 40.7 kD (Fig. 9C). It must be noted that nonspecific bands were also present at the 60-75kD region. Taken together these results showed that the *in-silico* data was reliable enough to support downstream assays, and that Newtic1 is indeed present within at the transcriptional and protein level.

5.3 Newtic1 Expression within a Subset of Erythrocytes

Tissue sections of the intact limb and blastema Stages I – III were collected for observation. Preliminary results showed that intact limb and Stage III blastemas immunoreactivity in cells resembling erythrocytes within muscle tissue (Fig. 10A), and inside blood vessels (Fig. 10B). This led to the reasoning that blood cells must be displaying some form of immunoreactivity; therefore blood smears were made and blood components were stained with Wright Geimsa staining to analyze and catalog the different cell types (Fig. 11). These staining results showed histological characteristics of erythrocytes throughout their various stages of maturation (Fig. 11A) as well as lymphocytes, eosinophils, and neutrophils (Fig. 11B). The proportion of normoblasts in all blood cells was 83-94% (n=9). Normoblasts were divided into basophilic normoblasts (BpNobs) and polychromatic normoblasts (PcNobs). BpNobs are an immature state of normoblasts, which are characterized by their oblate spheroid shape with a big round polychromatic nucleus and a narrow

cytoplasmic space. WG staining gave the cytoplasm of PcNobs a blue hue. PcNobs are defined as normoblasts in a transitional to mature state. The proportion of BpNobs and PcNobs in all normoblasts was less than 2.2% (1.1 ± 0.3%, n=9) and 97.8-100% (98.9 ± 0.3%, n=9), respectively. During the development of PcNobs, they change shape, becoming flattened ellipsoid (oval/oblong) and their nucleus becomes more compact. Concurrently, their cytoplasmic space gradually increases. The cytoplasmic stain also changed from grey to pink/orange as they matured while synthesizing hemoglobin (Fig. 11A). For this study, PcNobs were subdivided into early, intermediate and late stages: PcNobs at intermediate and late stages, which looked similar in morphology, were grey and pink/orange in color with the cytoplasmic stain, respectively. PcNobs at an early stage had a larger and rounder nucleus, and had less cytoplasmic space that was stained blue. However, in experiments in where immunocytochemistry was carried out using blood cell suspensions, PcNobs was divided just into two groups (early and intermediate/late) because it was difficult to differentiate between PcNobs at intermediate and late stages according to their morphological characteristics only. The proportion of early PcNobs and intermediate/late PcNobs in all PcNobs was 22.1 ± 2.2% (n=9) and 77.9 ± 2.2% (n=9), respectively. In particular experimental conditions where almost all PcNobs became slightly swollen and transparent, a small number of PcNobs was occasionally recognized at a late stage whose shape and color were preserved, and that never showed Newtic1 immunoreactivity. These cells are presumably in a mature state, corresponding to orthochromatic normoblasts (OcNobs). It was estimated that the incorporation of such presumptive OcNobs into intermediate/late PcNobs was less than 3.8% (n=3). Consequently, the ratio of normoblasts in the adult newt was roughly BpNobs : early PcNobs : intermediate/late PcNobs (OcNobs) = 1 : 22 : 77 (<3.8).

Having identified and cataloged the blood cell components, immunostaining was then carried out (Fig 12). Blood cell suspensions were stained with anti-Newtic1. Wright-Geimsa stain of the cell suspension showed consistent results as Figure 11 (Fig. 12A). Immunostaining with Newtic1 shows that among all the blood components; nucleated erythrocytes, particularly, PcNobs; were stained positively along the equatorial plane of the cell. These cells, under the immunostained condition; appear to have swollen and become transparent. Interestingly, fully matured erythrocytes were not displaying any form of staining around the cell's equatorial plane, which are presumably the Orthochromatic normoblasts, On (Fig. 12B). Obtaining cDNA from blood samples showed presence of Newtic1 transcripts being amplified by PCR (Fig. 12C). Western blot analysis was also able to detect Newtic1 protein at the 40.7Kd band (Fig. 12D). No other blood cell type displayed any form of immunoreactivity to Newtic1 antibody.

5.4 Newtic1+ cells Form Aggregates with Monocyte Cells in Peripheral Circulating Blood

Transitioning from blood smears, to the detection of Newtic1 within actual organ tissue; it has been known that newt blood cells are produced in the spleen (Jordan et al., 1930), and then released into the circulatory system for further maturation. This led to the speculation that vast quantities of Newtic1 should be present in splenic tissue of adult newts. Therefore tissues were collected, sectioned, and immunostained with Newtic1, and anti-vimentin antibody, which is an indicator for monocyte cells, and fibroblastic cells, which may also serve for detection of a regenerative response. As shown in Fig. 13A, the results showed Newtic1+ cells were present in blood within the splenic tissue and within the main splenic artery (Fig. 13A′). Surprisingly, in addition to those polychromatic normoblast cells having Newtic1+ staining, it was found that these

cells also appeared to clump together, typically around 1 to 2 vimentin+ cells as seen in Fig. 13 A′, A″.

To determine which cells were stained with Vimentin and whether or not this pattern was an artifact of stain, fixed blood smears were prepared, and double stained with Newtic1/Vimentin antibodies. Fig. 14A displays an aggregate of Newtic1+ PcNobs accumulating in a clump, (hereby referred to as *EryCs; Erythrocyte clump*) surrounding a Vimentin+ (having high immunoreactivity) cell, hereby known as *EryC-monocyte complex*. It is important to note that not all erythrocyte cells display Newtic1 signal including PcNobs; to these cells they are hereby referred to as Newtic1- cells (Fig. 14A). To identify if the Vim+ cell was a monocyte, comparative observations were performed with regarding size and morphology (Fig. 14B-D). Hematoxylin staining as well as α-esterase staining was also performed on the same kind of blood smears (Fig. 14C,D). Results showed monocytes were displayed a grainy black appearance characteristic of the stain, and displayed the same size as the cataloged cells. These EryC-monocyte complexes were often observed within the major blood vessels of the spleen, although seldom observed within splenic tissue. It is important to note that Newtic1+ PcNobs are present within splenic capillaries/tissues, but as free cells without any monocyte in the vicinity (Fig. 13A′). These EryCs appear to be assembling upon entering the major blood vessels, when they mix in with other blood cell components, along with Newtic1- cells.

5.5 EryCs are Newly Formed in the Limb Stump and Gradually Accumulate in the Distal Blastema

Having identified which cells express Newtic1, and detected these novel EryC clumps, it is necessary to elucidate their expression pattern on regenerating limb tissue. Intact limb tissue,

and Stage I - III regenerating tissues of adult newts were analyzed. Fig.15, comprehensively shows the overall expression of EryCs as early limb regeneration progresses. All regenerating samples were observed after amputating the mid-forearm of the right forelimb, and left to regenerate till the adequate stage was reached. In regards to intact limb tissue (0 DPA), after amputating, the sample was soon harvested and processed for fixation, and sectioned accordingly. During this stage, EryCs were hardly observed at the amputation site as well as within the muscle tissues in the underlying proximal region (Fig. 15). Vim+ cells and fibroblasts can be seen in small quantities at the periphery dermal region. EryCs can still be observed in the major arteries. Moreover, no other cell type or tissue was found to display any form of Newtic1 immunoreactivity. At stage I (3 DPA – 5 DPA) the wound epidermis (WE) was formed and covered the wound site, growing from the epidermal tissue located at the wound edge. During these stages, a large volume of monocytes accumulated in the space between the WE and the initial amputation site, flowing in from a blood vessel (Fig. 16A). This accumulation of monocytes is a major contributor to the early blastema that will begin to grow. Various monocytes can be observed to have extensions from their cell body, and were localized at the distal stump of the amputated tissues (i.e. muscle tissue) (Fig. 16B). One possibility for these extensions could be that these monocytes are differentiating into macrophages. When observing the muscle tissue proximal to the amputation stump, Newtic1+ PcNobs were found to be accumulated in the capillaries in between the muscle fibers. More specifically, these cells were not displaying a clump formation, but rather free-cell. To note, during stage I, a small portion of EryCs were able to be detected on the dorsal region. Interestingly, these EryCs seemed not to be accompanied by monocytes, and showing light immunoreactivity to Newtic1 antibody (Fig. 16E). Once the emerging blastema begins to protrude (Fig.15, stage II denoted by a P) notably at stage II (14DPA), EryCs appeared to accumulate at the distal portion

of the blastema protrusion. More defined EryCs can be observed in the proximal region of the blastema, and also in the non-regenerating region of the muscle, so as to be migrating from the non-regenerating region to the blastemal protrusion. At the same time, Vim+ cells in the blastema have decreased drastically. As the blastema protrusion continues to extend, the number of EryCs accumulated through the distal blastema, whilst at the same time, the number of EryC that had been seen previously in the proximal region, were disappearing (Fig. 15– Stage III, Fig. 16B, C). It must be noted that during this growth protrusion period, some EryCs were showing Vim+ monocytes next to them, despite the drastic decrease in overall Vimentin immunoreactivity throughout the blastemal tissue (Fig. 16C). Providing a statistical profile of the cell count of Newtic1+ PcNobs and Vimentin+ cells with respect to the overall cell count; there is a notable change in cell profile and behavior from stage I to stage III (Fig. 16D). It has been known that macrophages do accumulate at the blastema stemming from the traumatic injury response (Godwin et al. 2013). Lastly, it must be taken into consideration, that at stage III (27 DPA) (Fig. 16F), large vessels at the proximal region of the amputation plane, large vessels showed Newtic1+ cells and clumps, indicating some form of reestablishment of the 0 DPA physiological condition.

As mentioned previously, EryCs that were formed throughout Stage I - II, appeared without any signs of having any interaction with monocytes and also displayed light immunoreactivity. Since monocyte-less EryCs have not been seen before in other tissues, it was necessary to assess the origin to which these particular clumps were originated from. As we can observe in Fig. 16E, at stage I-5DPA, Newtic1 immunoreactivity was present at low levels, in a large number of PcNobs that had accumulated in dilated blood capillaries at the stump region. EryC-monocytes complexes seemed to only be observed in the large blood vessels. Interestingly, observing the number of Newtic1+ cells within the large blood vessels (amputated tissue sample and comparing between

non regenerating tissue), that the proportion of Newtic1+ PcNobs does not change (Fig. 16F). This may indicate that these PcNobs form at the blastemal stump region, independently of the presence of EryC-monocyte complexes that circulate within the main blood vessels. It was also observed that at Stage III blood, a number of EryCs-monocyte complexes were shown to be found throughout thick blood vessels in the stump region. This gives an indication that blood vessel diameter has restored into its original state after the inflammatory response ended. This will enable the EryCs in the capillaries to enter into the circulatory system.

To address how EryCs migrate from the proximal stump region into the distal blastemal protrusion, I reason that it must be via the development of the newly regenerating blood vessels, as these blood vessels follow a similar pattern to Peadon et al, 1966, in which they characterize the newly fromed limb throughout the regenerative process. Fig. 17A-D, shows EryCs have accumulated at the distal tip of the blastema, following capillary network, from the main body of the blastemal tissue. As the blastemal protrusion further developed, emerging blood vessels would fuse together creating more complete vascularization, with small ventricles at the fusion points (Fig. 17A'). Those Newtic1+ cells that would pass along the emerging vessels would accumulate at these ventricles, to form larger aggregates. The presence of EryC-monocyte complexes in more developed samples like late bud blastemas (38 DPA) (Fig. 17 B-E) may show that natural blood circulation has restarted with the formation of vascular networks. Interestingly, as the regenerating process enters the late blastema/palette stage, digits begin to form, and Newtic1+ PcNobs were appearing to show an evident decrease in size and overall quantity (Fig. 17C). Observing the region proximal to the amputation plane, the overall pattern of Newtic1 expression had changed to that similar to normal tissue, where EryCs were accompanied by monocytes (Fig. 17D). Moreover, the

muscular tissue present in proximity of the initial amputation plane appears to display similarities with normal tissue, due to the lack of overall immunoreactivity of Newtic1 and Vimentin.

5.6. EryC Presence on the Blastema is Specific to the Terrestrial Life-Stage

Apart from EryCs being expressed in the peripheral blood of the adult terrestrial-stage, I investigated whether larval newts have the same immunoreactivity within the blood and regenerating tissue. It is known that larval amphibian blood, generally originates from the kidneys, and shifts its production to the spleen after metamorphosis. Blastema samples of regenerating forelimbs at the mid bud blastema (stage III) (Fig. 18A-C) of larval newts (developmental stage 57-58), were collected and stained with Newtic1 and Vimentin. Fig. 18A displays Stage III blastema sample have no Newtic1+ cells within the developed protrusion area of the larval sample. A vast area of immunoreactivity with Vimentin is evident within the blastema, in contrast to the adult counterpart. Emphasizing on the composition of the blastema, it was found that blood vessels containing erythrocytes were present at the blastema protrusion however, they did not display any immunoreactivity toward Newtic1 antibody (Fig. 18B). Observing the proximal area of the same tissue sample reveals that there are a small number of Newtic1+ cells in thick blood vessels. Interestingly, these Newtic1+ cells did not display a form of aggregation, nor were there any signs of Vim+ immunoreactivity within monocytes (Fig. 18C). It must be important to note that the epidermal tissue of the blastema region did have several discrete structures showing some form of immunoreactivity to Newtic1, however these structures resembled more gland cells, and not within the blastema cell mass (Fig. 18A).

5.7 Erythrocytes Carry Secretory Molecules and May Deliver Them to the Growing Blastema in the Form of EryCs

To investigate potential functions or roles that EryCs were providing into the blastema, and the overall regenerative process; it was important to elucidate which genes were being expressed by erythrocytes. As my PCR results of Newtic1 blood suggest, adult erythrocytes are actively express genes even at their mature state. Examination of a gene profile of normal circulating blood via the mapping of mRNA-seq data (SRP034152; SAMN08574272–08574274) with the TOTAL transcriptome database revealed an abundance of genes coding for secretory molecules (Fig. 19A). This assay showed several growth factors that have been known to be implicated in the regenerative process: most notably cytokines (TGFβ-1, IGF-II, BMP2, PDGF-C, VEGF-C, nsCCN) and matrix metalloproteases (Col-a, Col-b, MMP3/10, MMP9, MMP21) (Bach et al., 2014, Bates et al., 2002, Dijke et al., 2007, Vinarsky et al., 2005, Wagner et al., 2017). To verify if these secretory molecules were indeed present within EryCs, cDNA samples were collected from purified blood (filtered and centrifuged adult erythrocytes; Fig. 19B), and PCR amplification of these was performed (Fig. 19C). Adequate PCR bands were able to be detected at the designated target bands. Among these, BMP2 and TGFβ-1 of the TGFβ superfamily were selected to be validated due to their essential implications in regeneration.

Performing immunohistochemistry on purified erythrocyte suspension, it was observed that both BMP2 and TGFβ-1 expression were present within the cytoplasm of PcNobs, double stained with Newtic1 (Fig. 20A-C). Looking in more detail of which developmental stage of PcNobs are positive to the double staining of Newtic1/Growth factors, results revealed that early PcNobs have TGFβ-1 or BMP2 immunoreactivity, and accounted for the majority of the cell count (statistical count in Fig. 20D,E description). Taking in consideration Newtic1 with these growth

factors, in regards to TGFβ-1 PcNobs with Newtic1+ immunoreactivity had more TGFβ-1 expression than those cells without Newtic1 expression, even as they developed into intermediate/late PcNob stages (Fig. D). It must be noted that in some cases, the intensity of immunofluorescence was sometimes higher at the equatorial plane of PcNobs, independent of the presence of Newtic1 expression also at the equatorial plane. Referring to BMP2, those early Newtic1+ PcNobs had statistically no difference with those on Newtic- early PcNobs. In regards to intermediate or late PcNobs, the data shows that the Newtic1+ PcNobs actually are displaying less immunoreactivity of BMP2 as opposed to the Newtic1- cells than those of Newtic1- PcNobs (Fig. 20E).

Assessing Newtic1/ TGFβ-1 or Newtic1/BMP2 co-localization within EryCs at the blastema lead to the following results (Fig. 21). The immunoreactivities of BMP2 or TGFβ-1 in the cytoplasm decreased as PcNobs were found moving into the blastema as EryCs. At the same time, as mentioned before, Newtic1 expression within those same PcNobs had increased. However, in the case of TGFβ-1, it was frequently observed in PcNobs, strong immunoreactivity in the form of dots spread across the equatorial plane, co-localized with Newtic1 expression (Fig 21A). Fig. 21B shows TGFβ-1expression in PcNobs circulating along the thick blood vessels near the elbow in the intact limb region. TGFβ-1immunoreactivity in these PcNobs was substantially the same as that observed in blood cell suspensions, though it was difficult to recognize differences in immunoreactivity between EryCs and free Newtic1-negative PcNobs. In regards to BMP2, immunoreactive dots were also observed but within the areas surrounding PcNobs, within the blood vessel space, and localized along the newly surrounding walls of the blood capillaries (Fig. 21C). It has been known that the TGFβ-1family are secreted as a delayed factor, protected by molecular protein cages that can bind to the extracellular matrices and micro fibrils across the

cell's membrane/cytoplasm which also contribute to the local concentration "spots" of these secretory molecules. Fig. 21D shows BMP2 expression in PcNobs circulating along thick blood vessels near the elbow (n = 3). The section was obtained from the same limb in (Fig. 21C). BMP2 immunoreactivity in PcNobs was substantially the same as that observed in blood cell suspensions. Observing both growth factors behaviors, it appears that these EryCs release TGFβ-1and/or BMP2 into the regenerating blood vessel, as they enter the region of the growing blastema. It is also important to note that neutrophils were also observable within these tissue samples in the vicinity of the emerging blood vessels. It appears these neutrophils have the capacity to also express BMP2 signaling throughout this process.

4. Discussion

It has long been known that the role of red blood cells is to function as a transport structure for the circulation of gases. Erythrocytes in mammals lose their nucleus and organelles to make space for oxygen transportation during maturation in the bone marrow in order to pass through the myriad network of capillaries and tissues. Aside from this primary function, previous studies have shown that erythrocytes may be involved in other functions such as hydrogen sulfide production, or immune response (Darley-Usmar et al, 2007, Giger et al. 2015). Mammalian nucleated erythrocytes or normoblasts are not liberated onto the circulatory system, until de-nucleation has occurred. On the other hand, non-mammalian vertebrates, such as amphibians, retain nucleated erythrocytes even until the cell's maturation (Claver et al. 2009, Giger et al. 2015). Currently, little is known as to the physiological roles and molecular involvement of homeostatic regulations as to why these organisms retain their nucleus, with the only exception being oxygen transport. The results of this study may provide insight as to newly detected functions that erythrocytes can perform other than oxygen transport, such as delivery of regulatory molecules; whilst also

detecting novel behavior of erythrocyte cell aggregation which circulates in the blood, and which may provide a physiological role in adult newt limb regeneration.

This study was aimed to elucidate; via the analysis of transcriptomes, to filter and detect novel blastema cell-specific genes that are found only during the early regenerative process, and specific to Urodeles. Surprisingly, my study led to the detection of a novel gene found in all stages of PcNobs (not as the initially deduced blastema cells). Identification of *Newtic1* gene also led to the detection to EryCs, erythrocyte clumps that circulate the blood stream, frequently accompanied by Vim+ monocytes (Fig. 22A). It still remains unknown what triggers Newtic1 expression in specific kinds of PcNobs. One speculation may be monocytes due to their presence in EryCs that are circulating in the peripheral blood. As summarized in Fig. 22B, in regards to limb regeneration, after amputation - during stage I, where there is a high presence of monocytic cells within the space between the wound epidermis and the amputation plane; PcNobs present in the proximal stump region show mild expression of Newtic1. It may be possible that the influx of these monocytes is creating an environment rich in regulatory factors that are activating the PcNobs. It is still not determined what mediates the Erythrocyte clumps nor the activation of *Newtic1* in the first place. Having a theoretical protein conformation of a transmembrane that is located at the equatorial plane of the cell, and while having a relatively short extracellular domain (1 – 16 a.a.), it is possible to speculate that this protein may be part of a complex that mediates cell aggregation, or be induced; though more studies would be needed for elucidation. What may be inferred is that this protein is conserved between various salamander species, providing a glimpse as to conservative mechanisms of regeneration at least within this clade.

Regarding Newtic1+ PcNob or EryCs role in early limb regeneration also remains to be studied. As seen in Fig. 20, EryCs have the capacity to carry secretory molecules throughout the

bloodstream, whether in high amounts or small quantities. These secretory carries must be regulated in a highly specific manner, to induce the proper response exactly where, when, and how much is needed. It is of particular interest that many of the selected candidates expressed in the blood mapping, represented a group of angiogenesis contributing molecules as well as vascular development, and remodeling (TGFβ-1, IGF-II, BMP2, PDGF-C, VEGF-C, and matrix metalloproteases) (Dijike, et al, 2007, Ucuzian et al, 2010). As limb regeneration commenced and progressed through the stages, EryC distribution pattern expression intensity would change together, within the blastema protrusion. Because of this, it can be said that EryCs are forming and entering the blastema protrusion via the formation of the new forming blood vessels. It must be noted that EryCs in themselves do not particularly contribute to the formation of the newly formed limb, but rather may have a role as signal delivery. As the vessels extend and fuse together in the blastema, EryCs begin to circulate within the peripheral blood.

Assessing the newt's ability to express Newtic1 in adults, it was fundamental to assess whether Newtic1+ is also present in larval blastemas, and moreover expressed within larval blood. It is well known that the larval stages of amphibians have a strong ability to regenerate, in particular limb regeneration (comparing aquatic larval life stage against the terrestrial adult life stage). Recent studies on *C. pyrrhogaster* and *A. mexicanum* showed that regenerating muscle tissue after limb amputation was restored primarily from satellite cells which are attached to muscle fibers (Tanaka et al, 2016, Sandoval, 2018) whilst in adult limb regeneration, muscle is restored from the dedifferentiation of muscle cells after cellularization. Displaying such differences with muscle regeneration begs the question: Does larval newt limb regeneration also exhibit the same behavior as its adult counterpart? As seen in Fig. 18, this shows to be the case. EryCs accumulating in the blastema seems to be an adult specific phenomena. It is important to note that there were some

newtic1 immunoreactivity, on the wound epidermis in the regenerating larval limb. Many larval samples showed Newtic1 immunoreactivity with structures having similar morphology to gland cells located at the outer layers of the larval skin. While Newtic1 may have roles in the blood, it may also be a possibility of having additional roles during the larval stage.

In searching for possible functions or physiological roles of Newtic1+ erythrocytes, RNA sequencing was performed, and transcripts were mapped against the TOTAL transcriptome database. Obtaining those differentially expressed sequences, gave the opportunity to study potential candidates to elucidate what roles these Newtic1+ PcNobs, and EryCs may have, as seen in Fig. 19. However, due to a matter of availability, TGFβ-1 and BMP2 were the only candidates that could have been investigated. A recent *in-vitro* on BMPs suggested that serum proteases such as thrombin and plasmin may promote cell cycle re-entry of dedifferentiating skeletal muscle fibers of adult newt limbs. Additionally, it is known that matrix-metalloproteases such as Col-a, MMP3/10, and MMP9 are necessary for blastema formation, but it is still unclear which cells are responsible for their secretion. This study may provide some insight as to the distribution of matrix metalloproteases and which cells are responsible for delivery (Fig. 21).

The most highly expressed secretory molecules was nsCCN gene. This molecule is a new member of the CCN family growth factor found in Urodeles, and recent studies show that this secretory molecule is involved in regeneration. In this context, endocardial cells localized at the damaged region express nsCCN inducing cellular repair. Comparing the mapping data collected here, these results showed nsCCN had an approximately 10 fold increase than the other secretory molecules. Due to this, PcNobs and/or EryCs appear to be likely candidates to provide this molecule to injured regions such as a wound stump. It is important to note that not only are these molecules secreted for physiological responses to erythrocytes/blood capillaries, but may also

affect mesenchymal cells within the blastema; due to the dilation of blood capillaries which can be regulated. Interestingly, neutrophils were also observed within the mesenchymal tissue of the blastema, possibly triggered as a response from the secretory molecules.

Newts have a masterful method to regenerate body parts and tissues. The exact mechanisms to perform this ability is still largely unknown. Identifying new genes and possibly novel molecular relationships may reveal new ways in which common cellular pathways may contribute to the regenerative process, such as what we see in this study summarized in Fig. 22. More vigorous studies in the future are needed to fully understand the extent to which the Newtic1+ cells contribute to the blastema, and moreover elucidate the mechanism that enables the newt to efficiently regenerate. Studies on blood serum on blastema cell cultures are needed to truly elucidate the functions of Newtic1, and assess whether or not it is vital to limb regeneration. Furthermore, conditionally knocking down, or over expressing Newtic1 can provide valuable insights on regeneration is performed.

7. Acknowledgements

First and Foremost, I would like to express my deepest gratitude to my Graduate School Advisor, Prof. Chiba Chikafumi, for the continuous support and guidance throughout my Ph.D study, for his kindness, motivation, and immense knowledge that you always share. I will forever appreciate all our discussions related to Newtic1, and the direction in which newtic regeneration is headed. I would also like to thank my lab members for their kind feedback,and support, that made this whole stay in Japan, and the lab, easier and welcoming.

Secondly I would like to thank Prof. Fubito Toyama, for his invaluable input and construction regarding many of the transcriptomes, raw data processing, and the initial perl script for subtraction of the normal limb components against the blastema transcriptome. Much of this research would not have been accomplished without your kind input and advice. Thank you greatly for your help throughout this entire study.

I deeply thank the thesis reviewers for their kind and insightful feedback, to create the final version of this thesis. Your challenging questions enabled me to think even deeper, and helped broaden my scope within this topic.

I thank the Japanese Government for granting me the MEXT Scholarship; Without this kind gift, none of this exciting research would have been possible. To this I give my kindest thanks. I would like to thank my dearest family, whom gave me constant support throughout this entire study, motivating me in good times and bad. Thank you.

Lastly, I give my warmest thanks to my wife, Nora. It is because of you, that I was able to endure this journey now and forever. My success was in a large part due to you unconditional love and support. I thank you for all eternity.

8. References

Abdullayev, I., Kirkham, M., Björklund, Å. K., Simon, A. & Sandberg, R. A reference transcriptome and inferred proteome for the salamander Notophthalmus viridescens. *Experimental Cell Research* **319,** 1187–1197 (2013).

Alvarado, A. S. & Tsonis, P. A. Bridging the regeneration gap: genetic insights from diverse animal models. *Nature Reviews Genetics* **7,** 873–884 (2006).

Bach, L. A. Endothelial cells and the IGF system. *Journal of Molecular Endocrinology* **54,** (2014).

Bates, D. & Harper, S. Regulation of vascular permeability by vascular endothelial growth factors. *Vascular Pharmacology* **39,** 225–237 (2002).

Carlson, M. R. J., Bryant, S. V. & Gardiner, D. M. Expression ofMsx-2 during development, regeneration, and wound healing in axolotl limbs. *The Journal of Experimental Zoology* **282,** 715–723 (1998).

Carter, C., Clark, A., Spencer, G. & Carlone, R. Cloning and expression of a retinoic acid receptor β2 subtype from the adult newt: Evidence for an early role in tail and caudal spinal cord regeneration. *Developmental Dynamics* **240,** 2613–2625 (2011).

Casco-Robles, M. M., Yamada, S., Miura, T., Nakamura, K., Haynes, T., Maki, N., Rio-Tsonis, K. D., Tsonis, P. A. & Chiba, C. Expressing exogenous genes in newts by transgenesis. *Nature Protocols* **6,** 600–608 (2011).

Casco-Robles, M. M., Islam, M. R., Inami, W., Tanaka, H. V., Kunahong, A., Yasumuro, H., Hanzawa, S., Casco-Robles, R. M., Toyama, F., Maruo, F. & Chiba, C. Turning the fate of reprogramming cells from retinal disorder to regeneration by Pax6 in newts. *Scientific Reports* **6,** (2016).

Casco-Robles, M. M., Miura, T. & Chiba, C. The newt (Cynops pyrrhogaster) RPE65 promoter: molecular cloning, characterization and functional analysis. *Transgenic Research* **24,** 463–473 (2014).

Casco-Robles, R. M., Watanabe, A., Eto, K., Takeshima, K., Obata, S., Kinoshita, T., Ariizumi, T., Nakatani, K., Nakada, T., Tsonis, P. A., Casco-Robles, M. M., Sakurai, K., Yahata, K., Maruo, F., Toyama, F. & Chiba, C. Novel erythrocyte clumps revealed by an orphan gene Newtic1 in circulating blood and regenerating limbs of the adult newt. *Scientific Reports* **8,** (2018).

Chiba, C., Yamada, S., Tanaka, H., Inae-Chiba, M., Miura, T., Casco-Robles, M. M., Yoshikawa, T., Inami, W., Mizuno, A., Islam, M. R., Han, W., Yasumuro, H., Matsumoto, M. & Takayanagi, M. Metamorphosis Inhibition: An Alternative Rearing Protocol for the Newt,Cynops pyrrhogaster. *Zoological Science* **29,** 293–298 (2012).

Chiba, C. Strategies for Retinal Regeneration in Vertebrates: from Fish to Human]. *Zoological Science* **22,** 1373–1376 (2005).

Christensen, R. N., Weinstein, M. & Tassava, R. A. Expression of fibroblast growth factors 4, 8, and 10 in limbs, flanks, and blastemas ofAmbystoma. *Developmental Dynamics* **223,** 193–203 (2002).

Christensen, R. N., Weinstein, M. & Tassava, R. A. Fibroblast growth factors in regenerating limbs ofAmbystoma: Cloning and semi-quantitative RT-PCR expression studies. *Journal of Experimental Zoology* **290,** 529–540 (2001).

Claver, J. A. & Quaglia, A. I. Comparative Morphology, Development, and Function of Blood Cells in Nonmammalian Vertebrates. *Journal of Exotic Pet Medicine* **18,** 87–97 (2009).

Dijke, P. T. & Arthur, H. M. Extracellular control of TGFβ signalling in vascular development and disease. *Nature Reviews Molecular Cell Biology* **8,** 857–869 (2007).

Eguchi, G., Eguchi, Y., Nakamura, K., Yadav, M. C., Millán, J. L. & Tsonis, P. A. Regenerative capacity in newts is not altered by repeated regeneration and ageing. *Nature Communications* **2,** (2011).

Elewa, A., Wang, H., Talavera-López, C., Joven, A., Brito, G., Kumar, A., Hameed, L. S., Penrad-Mobayed, M., Yao, Z., Zamani, N., Abbas, Y., Abdullayev, I., Sandberg, R., Grabherr, M., Andersson, B. & Simon, A. Reading and editing the Pleurodeles waltl genome reveals novel features of tetrapod regeneration. *Nature Communications* **8,** (2017).

Eto, K., Eda, K., Hayano, M., Goto, S., Nagao, K., Kawasaki, T., Kashimura, H., Tarui, H., Nishimura, O., Agata, K. & Abe, S.-I. Reduced Expression of an RNA-binding Protein by Prolactin Leads to Translational Silencing of Programmed Cell Death Protein 4 and Apoptosis in Newt Spermatogonia. *Journal of Biological Chemistry* **284,** 23260–23271 (2009).

Eto, K., Eda, K., Hayano, M., Goto, S., Nagao, K., Kawasaki, T., Kashimura, H., Tarui, H., Nishimura, O., Agata, K. & Abe, S.-I. Reduced Expression of an RNA-binding Protein by Prolactin Leads to Translational Silencing of Programmed Cell Death Protein 4 and Apoptosis in Newt Spermatogonia. *Journal of Biological Chemistry* **284,** 23260–23271 (2009).

Giger, K. M. & Kalfa, T. A. Phylogenetic and Ontogenetic View of Erythroblastic Islands. *BioMed Research International* **2015,** 1–8 (2015).

Giguère, V., Ong, E. S., Evans, R. M. & Tabin, C. J. Spatial and temporal expression of the retinoic acid receptor in the regenerating amphibian limb. *Nature* **337,** 566–569 (1989).

Girich, A. S., Isaeva, M. P. & Dolmatov, I. Y. Wnt and frizzled expression during regeneration of internal organs in the holothurian Eupentacta fraudatrix. *Wound Repair and Regeneration* **25,** 828–835 (2017).

Hubbard, T. The Ensembl genome database project. *Nucleic Acids Research* **30,** 38–41 (2002).

Imokawa, Y. & Yoshizato, K. Expression of sonic hedgehog gene in regenerating newt limbs. *Wound Repair and Regeneration* **6,** (1998).

Inoue, R. & Nakatani, K. Changes in the Olfactory Response to Amino Acids in Japanese Newts After Transfer from an Aquatic to a Terrestrial Habitat. *Zoological Science* **27,** 369–373 (2010).

Islam, M. R., Nakamura, K., Casco-Robles, M. M., Kunahong, A., Inami, W., Toyama, F., Maruo, F. & Chiba, C. The newt reprograms mature RPE cells into a unique multipotent state for retinal regeneration. *Scientific Reports* **4,** (2014).

Iwata, T., Nakada, T., Toyoda, F., Yada, T., Shioda, S. & Kikuyama, S. Responsiveness of vomeronasal cells to a newt peptide pheromone, sodefrin as monitored by changes of intracellular calcium concentrations. *Peptides* **45,** 15–21 (2013).

Jordan, H. E. & Speidel, C. C. The hemocytopoietic effect of splenectomy in the salamander, Triturus viridescens. *American Journal of Anatomy* **46,** 55–90 (1930).

Kawakami, Y., Esteban, C. R., Raya, M., Kawakami, H., Marti, M., Dubova, I. & Belmonte, J. C. I. Wnt/beta-catenin signaling regulates vertebrate limb regeneration. *Genes & Development* **20,** 3232–3237 (2006).

Knapp, D., Schulz, H., Rascon, C. A., Volkmer, M., Scholz, J., Nacu, E., Le, M., Novozhilov, S., Tazaki, A., Protze, S., Jacob, T., Hubner, N., Habermann, B. & Tanaka, E. M. Comparative Transcriptional Profiling of the Axolotl Limb Identifies a Tripartite Regeneration-Specific Gene Program. *PLoS ONE* **8,** (2013).

Kon, S., Sato, T., Endo, D., Takahashi, T., Takaku, A., Nakauchi, Y., Toyama, F., Meyer-Rochow, V. B., Takayama-Watanabe, E. & Watanabe, A. Sperm storage influences the potential for

spontaneous acrosome reaction of the sperm in the newt Cynops pyrrhogaster. *Molecular Reproduction and Development* **84,** 1314–1322 (2017).

Koshiba, K., Kuroiwa, A., Yamamoto, H., Tamura, K. & Ide, H. Expression ofMsx genes in regenerating and developing limbs of axolotl. *The Journal of Experimental Zoology* **282,** 703–714 (1998).

Kumar, A., Godwin, J. W., Gates, P. B., Garza-Garcia, A. A. & Brockes, J. P. Molecular Basis for the Nerve Dependence of Limb Regeneration in an Adult Vertebrate. *Science* **318,** 772–777 (2007).

Kumar, A., Velloso, C. P., Imokawa, Y. & Brockes, J. P. The Regenerative Plasticity of Isolated Urodele Myofibers and Its Dependence on Msx1. *PLoS Biology* **2,** (2004).

Looso, M., Michel, C. S., Konzer, A., Bruckskotten, M., Borchardt, T., Krüger, M. & Braun, T. Spiked-in Pulsed in Vivo Labeling Identifies a New Member of the CCN Family in Regenerating Newt Hearts. *Journal of Proteome Research* **11,** 4693–4704 (2012).

Mccusker, C. D., Athippozhy, A., Diaz-Castillo, C., Fowlkes, C., Gardiner, D. M. & Voss, S. R. Positional plasticity in regenerating Amybstoma mexicanum limbs is associated with cell proliferation and pathways of cellular differentiation. *BMC Developmental Biology* **15,** (2015).

Mcewan, J., Lynch, J. & Beck, C. W. Expression of key retinoic acid modulating genes suggests active regulation during development and regeneration of the amphibian limb. *Developmental Dynamics* **240,** 1259–1270 (2011).

Monaghan, J. R., Athippozhy, A., Seifert, A. W., Putta, S., Stromberg, A. J., Maden, M., Gardiner, D. M. & Voss, S. R. Gene expression patterns specific to the regenerating limb of the Mexican axolotl. *Biology Open* **1,** 937–948 (2012).

Mutua, J., Jinno, Y., Sakata, S., Okochi, Y., Ueno, S., Tsutsui, H., Kawai, T., Iwao, Y. & Okamura, Y. Functional diversity of voltage-sensing phosphatases in two urodele amphibians. *Physiological Reports* **2,** (2014).

Nacu, E., Gromberg, E., Oliveira, C. R., Drechsel, D. & Tanaka, E. M. FGF8 and SHH substitute for anterior–posterior tissue interactions to induce limb regeneration. *Nature* **533,** 407–410 (2016).

Nakamura, K. & Chiba, C. Evidence for Notch signaling involvement in retinal regeneration of adult newt. *Brain Research* **1136,** 28–42 (2007).

Nakamura, K., Islam, M. R., Takayanagi, M., Yasumuro, H., Inami, W., Kunahong, A., Casco-Robles, R. M., Toyama, F. & Chiba, C. A Transcriptome for the Study of Early Processes of Retinal Regeneration in the Adult Newt, Cynops pyrrhogaster. *PLoS ONE* **9,** (2014).

Neff, A. W., King, M. W. & Mescher, A. L. Dedifferentiation and the role of sall4 in reprogramming and patterning during amphibian limb regeneration. *Developmental Dynamics* **240,** 979–989 (2011).

Nguyen, M., Singhal, P., Piet, J. W., Shefelbine, S. J., Maden, M., Voss, S. R. & Monaghan, J. R. Retinoic acid receptor regulation of epimorphic and homeostatic regeneration in the axolotl. *Development* **144,** 601–611 (2017).

Nowoshilow, S., Schloissnig, S., Fei, J.-F., Dahl, A., Pang, A. W. C., Pippel, M., Winkler, S., Hastie, A. R., Young, G., Roscito, J. G., Falcon, F., Knapp, D., Powell, S., Cruz, A., Cao, H., Habermann, B., Hiller, M., Tanaka, E. M. & Myers, E. W. The axolotl genome and the evolution of key tissue formation regulators. *Nature* **554,** 50–55 (2018).

Peadon, A. M. & Singer, M. The blood vessels of the regenerating limb of the adult newt,Triturus. *Journal of Morphology* **118,** 79–89 (1966).

Poss, K. D. Advances in understanding tissue regenerative capacity and mechanisms in animals. *Nature Reviews Genetics* **11,** 710–722 (2010).

Ragsdale, C. W., Petkovich, M., Gates, P. B., Chambon, P. & Brockes, J. P. Identification of a novel retinoic acid receptor in regenerative tissues of the newt. *Nature* **341,** 654–657 (1989).

Satoh, A., Nakada, Y., Suzuki, M., Tamura, K. & Ide, H. Analysis of scleraxis and dermo-1 genes in a regenerating limb ofXenopus laevis. *Developmental Dynamics* **235,** 1065–1073 (2006).

Satoh, A., Bryant, S. V. & Gardiner, D. M. Regulation of dermal fibroblast dedifferentiation and redifferentiation during wound healing and limb regeneration in the Axolotl. *Development, Growth & Differentiation* **50,** 743–754 (2008).

Shimokawa, T., Yasutaka, S., Kominami, R. & Shinohara, H. Lmx-1b and Wnt-7a expression in axolotl limb during development and regeneration. *Okajimas Folia Anatomica Japonica* **89,** 119–124 (2013).

Showalter, A. D., Yaden, B. C., Chernoff, E. A. & Rhodes, S. J. Cloning and analysis of axolotl ISL2 and LHX2 LIM-homeodomain transcription factors. *genesis* **38,** 110–121 (2004).

Simon, A. & Tanaka, E. M. Limb regeneration. *Wiley Interdisciplinary Reviews: Developmental Biology* **2,** 291–300 (2012).

Sousounis, K., Qi, F., Yadav, M. C., Millán, J. L., Toyama, F., Chiba, C., Eguchi, Y., Eguchi, G. & Tsonis, P. A. A robust transcriptional program in newts undergoing multiple events of lens regeneration throughout their lifespan. *eLife* **4,** (2015).

Spater, D. Wnt9a signaling is required for joint integrity and regulation of Ihh during chondrogenesis. *Development* **133,** 3039–3049 (2006).

Stewart, R., Rascón, C. A., Tian, S., Nie, J., Barry, C., Chu, L.-F., Ardalani, H., Wagner, R. J., Probasco, M. D., Bolin, J. M., Leng, N., Sengupta, S., Volkmer, M., Habermann, B., Tanaka, E.

M., Thomson, J. A. & Dewey, C. N. Comparative RNA-seq Analysis in the Unsequenced Axolotl: The Oncogene Burst Highlights Early Gene Expression in the Blastema. *PLoS Computational Biology* **9,** (2013).

Susaki, K. & Chiba, C. MEK mediates in vitro neural transdifferentiation of the adult newt retinal pigment epithelium cells: Is FGF2 an induction factor? *Pigment Cell Research* **20,** 364–379 (2007).

Takano, K., Obata, S., Komazaki, S., Masumoto, M., Oinuma, T., Ito, Y., Ariizumi, T., Nakamura, H. & Asashima, M. Development of Ca2 signaling mechanisms and cell motility in presumptive ectodermal cells during amphibian gastrulation. *Development, Growth & Differentiation* **53,** 37–47 (2011).

Tanaka, H. V., Ng, N. C. Y., Yu, Z. Y., Casco-Robles, M. M., Maruo, F., Tsonis, P. A. & Chiba, C. A developmentally regulated switch from stem cells to dedifferentiation for limb muscle regeneration in newts. *Nature Communications* **7,** 11069 (2016).

Tominaga, A., Matsui, M., Yoshikawa, N., Eto, K. & Nishikawa, K. Genomic Displacement and Shift of the Hybrid Zone in the Japanese Fire-Bellied Newt. *Journal of Heredity* **109,** 232–242 (2017).

Tominaga, A., Matsui, M. & Kokuryo, Y. Occurrence and Evolutionary History of TwoCynops pyrrhogasterLineages on the Izu Peninsula. *Current Herpetology* **34,** 19–27 (2015).

Tominaga, A., Meyer-Rochow, V. B., Okamoto, T., Kuriyama, T., Nishikawa, K. & Matsui, M. Origin and Genetic Uniformity of Introduced Population ofCynops pyrrhogaster(Amphibia: Urodela) on Hachijojima Island. *Current Herpetology* **35,** 64–68 (2016).

Tominaga, A., Matsui, M., Yoshikawa, N., Nishikawa, K., Hayashi, T., Misawa, Y., Tanabe, S. & Ota, H. Phylogeny and historical demography of Cynops pyrrhogaster (Amphibia: Urodela):

Taxonomic relationships and distributional changes associated with climatic oscillations. *Molecular Phylogenetics and Evolution* **66,** 654–667 (2013).

Torok, M. A., Gardiner, D. M., Izpisúa-Belmonte, J. C. & Bryant, S. V. Sonic Hedgehog (shh) expression in developing and regenerating axolotl limbs. *Journal of Experimental Zoology* **284,** 197–206 (1999).

Tsonis, P. A. & Fox, T. P. Regeneration according to Spallanzani. *Developmental Dynamics* **238,** 2357–2363 (2009).

Ueno, T., Ohgami, T., Harada, Y., Ueno, S. & Iwao, Y. Egg activation in physiologically polyspermic newt eggs: involvement of IP3 receptor, PLCγ, and microtubules in calcium wave induction. *The International Journal of Developmental Biology* **58,** 315–323 (2014).

Vinarsky, V., Atkinson, D. L., Stevenson, T. J., Keating, M. T. & Odelberg, S. J. Normal newt limb regeneration requires matrix metalloproteinase function. *Developmental Biology* **279,** 86–98 (2005).

Wagner, I., Wang, H., Weissert, P. M., Straube, W. L., Shevchenko, A., Gentzel, M., Brito, G., Tazaki, A., Oliveira, C., Sugiura, T., Shevchenko, A., Simon, A., Drechsel, D. N. & Tanaka, E. M. Serum Proteases Potentiate BMP-Induced Cell Cycle Re-entry of Dedifferentiating Muscle Cells during Newt Limb Regeneration. *Developmental Cell* **40,** (2017).

Weisrock, D. W., Papenfuss, T. J., Macey, J. R., Litvinchuk, S. N., Polymeni, R., Ugurtas, I. H., Zhao, E., Jowkar, H. & Larson, A. A molecular assessment of phylogenetic relationships and lineage accumulation rates within the family Salamandridae (Amphibia, Caudata). *Molecular Phylogenetics and Evolution* **41,** 368–383 (2006).

Yanagi, T., Ito, K., Nishihara, A., Minamino, R., Mori, S., Sumida, M. & Hashimoto, C. The Spemann organizer meets the anterior-most neuroectoderm at the equator of early gastrulae in amphibian species. *Development, Growth & Differentiation* **57,** 218–231 (2015).

Yokoe, M., Takayama-Watanabe, E., Saito, Y., Kutsuzawa, M., Fujita, K., Ochi, H., Nakauchi, Y. & Watanabe, A. A Novel Cysteine Knot Protein for Enhancing Sperm Motility That Might Facilitate the Evolution of Internal Fertilization in Amphibians. *Plos One* **11,** (2016).

Yokoe, M., Sano, M., Shibata, H., Shibata, D., Takayama-Watanabe, E., Inaba, K. & Watanabe, A. Sperm Proteases that May Be Involved in the Initiation of Sperm Motility in the Newt, Cynops pyrrhogaster. *International Journal of Molecular Sciences* **15,** 15210–15224 (2014).

Yokoyama, H., Ogino, H., Stoick-Cooper, C. L., Grainger, R. M. & Moon, R. T. Wnt/β-catenin signaling has an essential role in the initiation of limb regeneration. *Developmental Biology* **306,** 170–178 (2007).

Yoshikawa, T., Mizuno, A., Yasumuro, H., Inami, W., Vergara, M. N., Rio-Tsonis, K. D. & Chiba, C. MEK-ERK and heparin-susceptible signaling pathways are involved in cell-cycle entry of the wound edge retinal pigment epithelium cells in the adult newt. *Pigment Cell & Melanoma Research* **25,** 66–82 (2011).

9. FIGURES


A
B
C
D

Fig. 1. *Cynops pyrrhogaster*. A) Photograph of an adult Japanese fire-bellied newt, *Cynops pyrrhogaster*. **B – D)** Pictures display various tissues with the potential to regenerate. **B)** Tail and spinal cord. **C)** Cerebrum of newt undergoing enchephalectomy. **D)** Exposed heart to surgically remove cardiac muscle from the lower tip of the ventricle.

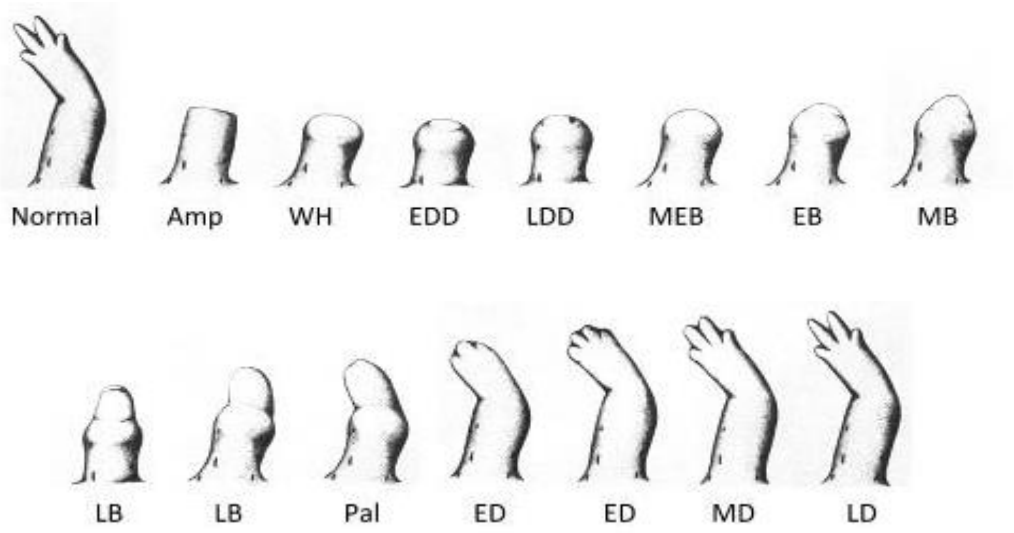
Normal
Amp
WH
EDD
LDD
MEB
EB
MB
LB
LB
Pal
ED
ED
MD
LD

Fig. 2. Stages of adult limb regeneration. After amputation, the wound site undergoes a series of stages until the formation of a newly ground functional limb. The stage abbreviations are as follows: WH – wound healing, EDD – early de-differentiation, LDD – late de-differentiation, MEB – moderate early bud blastema, EB – early bud blastema, MB – medium bud blastema, - LB late bud blastema, Pal – palette stage, ED - early digits, MD – medium digits, and LD – late digits [Modified from Iten and Bryant., 1973, and is used explicitly for explanatory purpose].

IMORI: The sequence resource for the Japanese fire bellied newt

http://antler.is.utsunomiya-u.ac.jp/imori/

Sample		Transcriptome No. of *IS*-transcripts (N50)
● Regenerating eyes after removal of the neural retina and lens		
Day 0-14	330,837,190	* 237,120 (2,737 b)
Day 20	74,256,628	135,463 (1,288 b)
Day 25	60,369,250	129,654 (1,509 b)
Day 30	28,424,810	102,378 (1,004 b)
Day 50	31,327,236	115,298 (1,159 b)
		172,275 (2,615 b)
● Normal lens	150,045,308	128,908 (1,113 b)
● Normal and regenerating brains	222,723,490	189,716 (3,156 b)
● Normal and regenerating hearts	80,755,634	119,520 (2,120 b)
● Limb blastema (Stage I - III)	99,532,656	105,467 (2,758 b)
● Normal limb	80,527,012	93,325 (1,676 b)
● Testis	113,518,996	105,841 (2,411 b)
● Testis (Apoptosis induction)	90,828,294	126,909 (1,844 b)
● Ovary	112,899,960	74,569 (3,212 b)
● Oviduct	114,673,672	* 113,084 (1,830 b)
● Olfactory epithelium & Vomeronasal organ	101,414,184	132,997 (2,189 b)
● Viscera (Lung, Intestine, Pancreas, Liver, Kidney)	169,436,506	127,099 (1,884 b)
● Whole embryos		
Stage 5 (16-cell stage)	114,500,038	93,067 (3,803 b)
Stage 18 (Neurula stage)	101,749,338	146,382 (2,478 b)
Stage 29 (Tail bud stage)	99,306,630	151,037 (2,824 b)
		260,963 (3,014 b)

De novo assemble by Trinity
697,670 contigs

Removal of 3,532 bacterial contigs

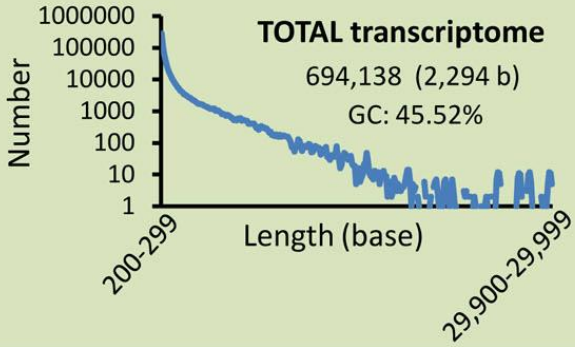

Fig 3. TOTAL transcriptome overview as found specifically in IMORI.

For the study of the Japanese fire-bellied newt *Cynops pyrrhogaster*, the Japan Newt Research Community (JNRC) opened the sequence resource site 'IMORI' to the public in 2014 (http://antler.is.utsunomiya-u.ac.jp/imori). Present here are all the individual transcriptomes assembled from the various tissues harvested. Taken together, all the raw sequences from these tissues were gathered together, and assembled into a comprehensive transcriptome database named 'TOTAL' (image adapted from Casco et. al, 2018).

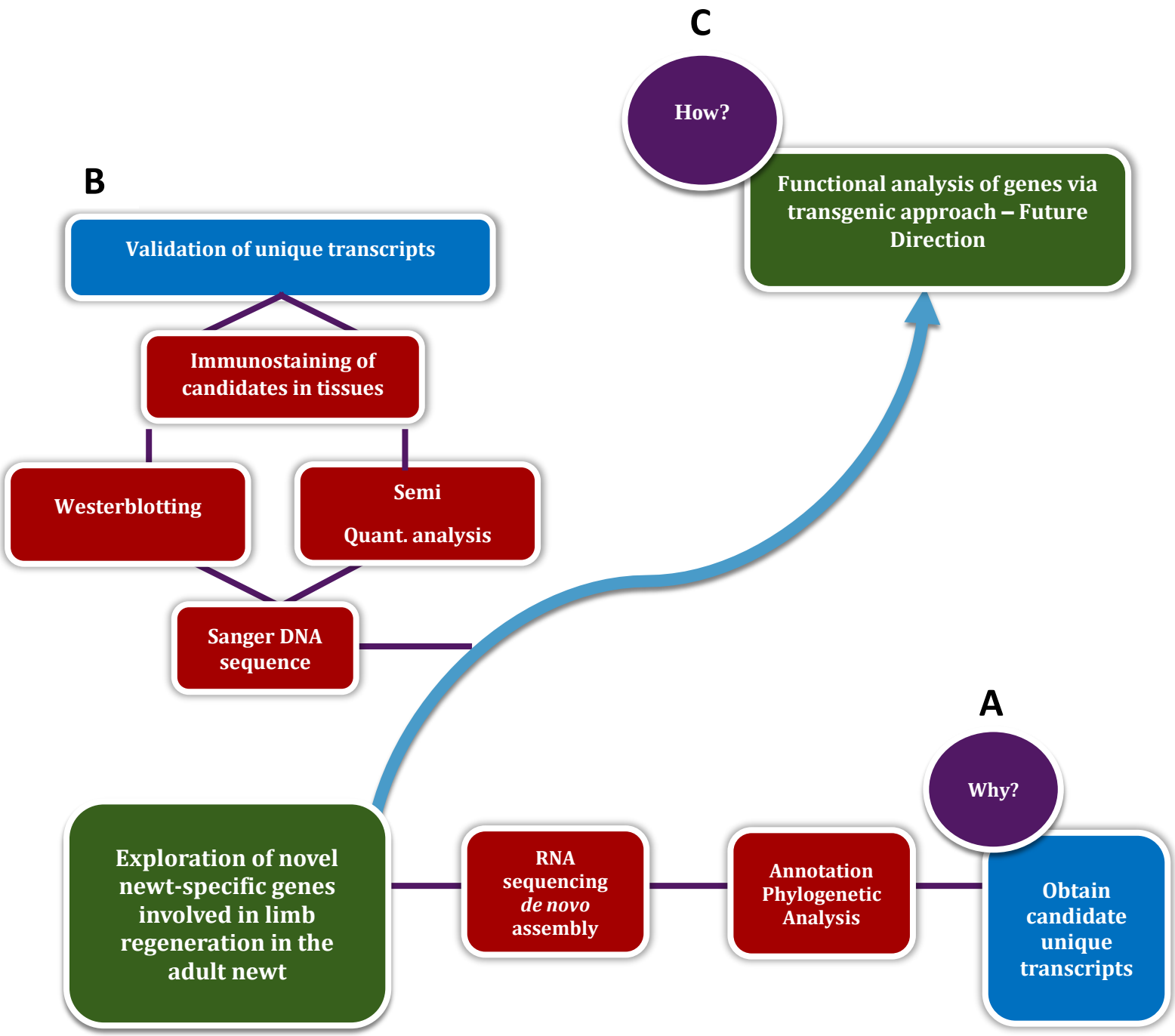
C
How?
Functional analysis of genes via transgenic approach – Future Direction
B
Validation of unique transcripts
Immunostaining of candidates in tissues
Westerblotting
Semi
Quant. analysis
Sanger DNA sequence
A
Why?
Exploration of novel newt-specific genes involved in limb regeneration in the adult newt
RNA sequencing *de novo* assembly
Annotation Phylogenetic Analysis
Obtain candidate unique transcripts

Fig. 4. Research flow Diagram.

This diagram is a representation of the flow of experiments to reach the ultimate goal for this study. **A)** The first set of work involved analyzing transcriptome data to obtain transcripts that are unique and expressed in limb regeneration, by the comparison of blastema transcriptomes against the normal limb transcriptome**. B)** Focuses more on validating if these *in silico* transcripts indeed present in cDNA, protein, and if mRNA/Proteins are actually localized within blastema tissues. Further analysis was to verify a particular expression pattern of thesis candidates during the early regenerative process. **C)** After confirmation of theses novel genes within the blastema, a functional analysis will be performed to knockdown these genes via shRNAi either using a CRE/LOXp recombinase system, or a CRISPR-CAS9 system.

Normal limb sample (NL)

Blastema sample (B)

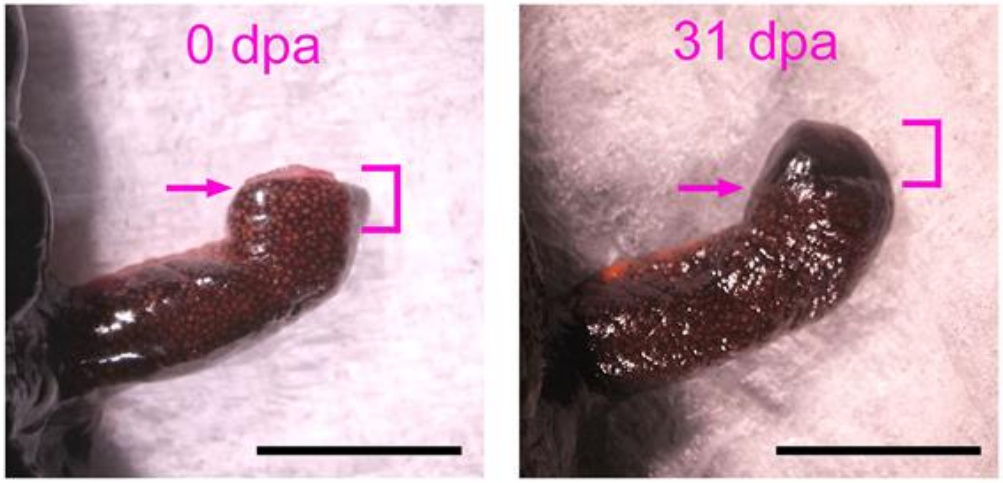

Fig 5. Tissue sample collected from 0 DPA and 31DPA for RNA extraction.

For normal limb (NL), tissues in the region up to 1.5 mm proximal to the amputation plane were harvested immediately after the limb was amputated in the middle of the right forearm (0 days post-amputation (DPA)). For the blastema (B), samples were harvested by sectioning the limb at the location of amputation. Limbs were allowed to regenerate until the desired stage had been reached. Samples were then harvested by a second incision at the base of the blastema. Scale bars, 5 mm (image adapted from Casco et. al, 2018).

.

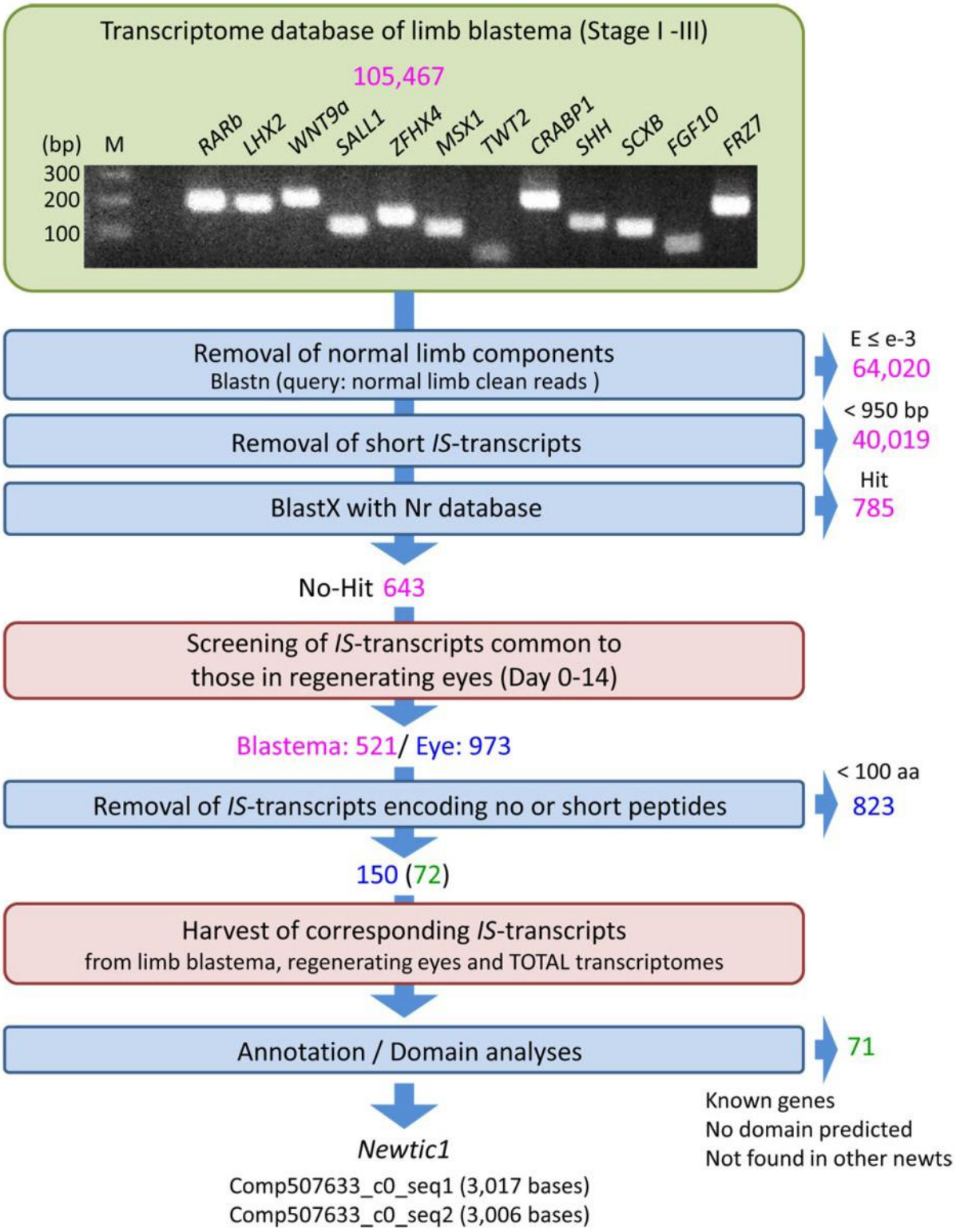
Transcriptome database of limb blastema (Stage I -III)
105,467
(bp)
M
300
200
100
RARb
LHX2
WNT9a
SALL1
ZFHX4
MSX1
TWT2
CRABP1
SHH
SCXB
FGF10
FRZ7
Removal of normal limb components
Blastn (query: normal limb clean reads)
E ≤ e-3
64,020
Removal of short IS-transcripts
< 950 bp
40,019
BlastX with Nr database
Hit
785
No-Hit 643
Screening of IS-transcripts common to
those in regenerating eyes (Day 0-14)
Blastema: 521/ Eye: 973
Removal of IS-transcripts encoding no or short peptides
< 100 aa
823
150 (72)
Harvest of corresponding IS-transcripts
from limb blastema, regenerating eyes and TOTAL transcriptomes
Annotation / Domain analyses
71
Known genes
No domain predicted
Not found in other newts
Newtic1
Comp507633_c0_seq1 (3,017 bases)
Comp507633_c0_seq2 (3,006 bases)

Fig 6. Work flow showing the screening of unique genes whose quantity of transcripts increased in the adult newt limb blastema.

Starting from the transcriptome (105,464 *IS*-transcripts) of the limb blastema, this transcriptome contained sequence information of genes that have been suggested to participate in limb regeneration (see the inset PCR results). I screened *IS*-transcripts (≥ 209 950 bases) whose expression might have been up-regulated in the blastema by subtracting normal limb components from the blastema transcriptome. Those transcripts containing short reads and Nr-annotated *IS*-transcripts were then filtered out, in resulting 643 *IS*-transcripts. From the remaining 643 No-Hit *IS*-transcripts, 72 candidate protein-coding genes whose *IS*-transcripts (150 in total) also existed in the transcriptome of regenerating eyes (Day 0-14) were screened. I collected *IS*-transcripts corresponding to the 72 candidate genes from the limb blastema, regenerating eyes and TOTAL transcriptomes, and manually screened unique candidate genes through Nr annotation and domain analysis (InterProScan sequence search; https://www.ebi.ac.uk/interpro/search/sequence-search). One sequence was finally obtained that also existed in other newt species, which were found in TOTAL (image adapted from Casco et. al, 2018).

A *Newtic1* (1,512 bp)

GCTCGTGTGAAACCTAAGAGAGAGAGGCAGCCGGACACCTGCAGTCGGCACAGGTGAGCAGCGCCGGCCTGGAGCAGCCTCCCC
TCCCGGGGCGATAGGCTGCAACGTGTCGAACACACTCCCCTTGGGCACCATACCCCAAGCTCCGCACAGAGCCGGGCTCGCTGAC
CTACTCACCTGCTGCTGGAGCTCATCCTCTGTGATACACCAGGCTCCGCGTGATGGCGGGCAGCCTGGAGCCAGCCATGGCCACTA
CCAGCTACTCCGCCTTCCTGTGGGCTCTGATGTCCACGGCCTCTATGGTATCCACTGTCGCCCTCCTCCTGCTGTGCGGATTGTGTA
GGCGCTTGAGGAAACAAGGATCACATTCCATAAGCGCAAGAAATGGCAGCCTCACCAGAGCACAAACAACACTCACTAAAGTTAC
TCAAAAAAATGAGGAGTTGCCAATGAATGGCACTAAGACGGTGGAAGGAATAGAAAATGGAGCCTTTTCAGCTTCTGAACCAGT
GGATCCATCAGAGCCACAAGTAGAACTTCCCGTGGATGTGCAGACATCACGCAGGTCTCCCGATTCAAAGAGAGCTTCCCAAAAT
AAAACCCTGCAGGGACCCCAAGAATCCTTAAAGCACAGGAGGCTTCCAAGCATCCCTCACATCATGCTCAACCAACCCGACAATGA
GCGAAACTCAGGGGTGCCGATGCAGAGACCTACATTTCAACCTCCAGAGCCACCAACGTACGAGGAGGTGCATGGTGGGAAAGC
CGCCGTGGAATCCGGACCTCCAGAGAGGGCAGTGGGCGGTGGACTCTCTCAGCGAGTAGGCCCTATGCATGAAAGTTGGATTGG
TGATGATGAAGAATGGCCGGCTGCCCCGCCTCTGACTCTTTTCGACCAACCCTTTGAAAATGTATATACAGATTTGAAAAATGAAA
GTATTGCTACCCTAAAAGATCAGCCAATCATTGTGCCAACTGTTGACTCTGCTGGTACGCAGAAAAGCTCACCGCAGGCCACGGCC
TCCGTCGGAGTGGAGCCTCATGAGGAAAATTCAACTTCCATCCCAGCACCATTATCATGGCGGTTTCACTTAGCCCTTGCATCTAAC
ACTGAAGATAACACAGCTGTTCAAGACCCGACACTGACCGGTCTATATAGTAAGGTAAAGAAGAGCACTAAGCGCCCCTTTTCTTT
ACCATCGTCCACCTTGGAAGATCCCTTAAAGGTTGAAGACGATGTGCCACCGCCTGTGCCAGTAAAGCAGTTTGATATCGAAGAG
GATCTGTCCACTCAGAATCAGGACATCGAGGACCCATTGCCGCCACCACCCATCCTATTAATTAACTGATCCATGGGGTTGGTGAA
TTCACTGAGACCTGTAGCAGAATATTGTGCATGGGGGCCAATCTCCGAAGGGTCTGTGAAATCATGGATAGAACAGGAGTCTTTG
GAATGATCTCTTATTGCCATCAGTCACACTGCATACTTTGCACAATGTAATCCTCACAAGT

B Predicted protein (375 amino acids)

MAGSLEPAMATTSYSAFLWALMSTASMVSTVALLLLCGLCRRLRKQGSHSISARNGSLTRAQTTLTKVT
QKNEELPMNGTKTVEGIENGAFSASEPVDPSEPQVELPVDVQTSRRSPDSKRASQNKTLQGPQESLK
HRRLPSIPHIMLNQPDNERNSGVPMQRPTFQPPEPPTYEEVHGGKAAVESGPPERAVGGGLSQRVG
PMHESWIGDDEEWPAAPPLTLFDQPFENVYTDLKNESIATLKDQPIIVPTVDSAGTQKSSPQATASVG
VEPHEENSTSIPAPLSWRFHLALASNTEDNTAVQDPTLTGLYSKVKKSTKRPFSLPSSTLEDPLKVEDDVP
PPVPVKQFDIEEDLSTQNQDIEDPLPPPPILLIN

C

Fig. 7. Newtic1 Sequence.

A) Newtic1 sequence is present in both the genome (displaying no introns) and cDNA. Red font area indicates the open reading frame and black fonts indicates the UTR sequence. Underlines indicate the sequences corresponding to the primer sets used for PCR analysis. Black underline indicates long primer set, while red underline indicates short primer set. **B)** Amino acid sequence was deduced by Expasy translator. Underline in the amino acid sequence indicates the epitope sequence of the Newtic1 antibody. **C)** Structure of the theoretical protein, with the following sections: 1-15, Non- cytoplasmic domain; 16-40, Transmembrane domain; 41 -375, Cytoplasmic domain (image adapted from Casco et. al, 2018).

A

TM domain

```
Cynops pyrrhogaster          MAGSLEPAMATTSYSAFLWALMSTASMVSTVALLLLCGLCRRLRKQGSHSISARNGSLTR
Notophthalums viridescens    MAGSMEPAMATISLSTFQWALMSMATIVVTVLLVLLCGLCNCLKKQGKHSMSGGNGGISR
Pleurodeles waltl            MAGSLEPAMATTIHSTFQWALMSIATMVPTVLLLLLCGFCLRLRKKRAHSLRERNGSLNR
Ambystoma mexicanum          MAGSLASGAASG---SFQWALLSVVTLVPTILLLLFCGFCRRFSKHRSHSLHASNG-NAR
                             ****: .. *:    :* ***:* .::* *: *:*:**:*  : *:  **:   **   *

Cynops pyrrhogaster          -AQTTLTKVTQKNEELPMNG-TKTVEGIENGAFSASEPVDPS--------------EPQV
Notophthalums viridescens    GTTTTLTKVTHKKEDLPVNG-TKTVNGIENGAYSASEPMEQSKTSAEMN-SFGIGTEEGA
Pleurodeles waltl            -APTTLTKVTQKKDDLPVYG-TKTVNGIENGAFSASEREEQSK-----------------
Ambystoma mexicanum          TNSTALTGHTQKKDGVTLNGGDKAKEGIVNGSFSPDKALEEAKTQPEMNGRAAIVAEEVT
                                *:**  *:*:: :.: *  *: :** **::*..:  : :

Cynops pyrrhogaster          ELPVDVQTSRRSPDSKRASQNKTLQGPQESLKHRRLPSIPH-----IMLNQPDNERNSGV
Notophthalums viridescens    FLPVDLQTSRGSPDSRRASQNKTLQEPQESFKHRRLPSIPH-----TMLEQPNSERNAGV
Pleurodeles waltl            --TPVEQTSHGSSDSRRASQNKTLQGPQESLKHRRLPSIPH-----TMLDQPNSEQSSGV
Ambystoma mexicanum          SRTREQEVARGFGDSAWASTSGNLQAPQESFKHRKLPSIPHALAHIDLVNQPDSGKNSEE
                               .   :.::   **  ** . .** ****:***:******      :::**:. :.:

Cynops pyrrhogaster          PMQRPTFQPPEPPTYEEVHGGKAAVESGPPERAVGGGLSQRV-GPMHESWIGDDEEWPAA
Notophthalums viridescens    LMRRPTVQPPEPPTYEEVHVEKAVVDARTPEGGVSGGLARPL-GPMHESWIDDDEEWPAA
Pleurodeles waltl            LVRRPTVQPPAPPTYEEVHVGKATDEAQPPEGTVGGRLVMRS-GPMHESWIDNDEEWPAA
Ambystoma mexicanum          ELQKTRADPAEPPTYEELPVGQSIFEDIPLEGAVGGLSSHDRQGLTHESWIDVEEEWPAA
                              :::.  :*. ******:   ::  :  . *  *.*       *  *****. :******

Cynops pyrrhogaster          PPLTLFDQPFENVYTDLKNESIATLKDQPIIVPTVDSAGTQKSSPQATASVGVEPHEENS
Notophthalums viridescens    PPLTLFDQPLENVYSELKNESMAALKDQ----PTVDFAGTQKSSPQATVSVGEEPHIENS
Pleurodeles waltl            PPLTLFDQPPENVYTDLRNESMAAIGDQ----PTIDSAGTLESSSQATASVREEANDKDS
Ambystoma mexicanum          PPLTLFNQPVENLYSDLSKSSPSHQAVS----VPIVTEERPPEASTPNGAAGEGRDPATP
                             ******:** **:*::* :.* :    .     .:       .:. .. :.    .   .

Cynops pyrrhogaster          TSIPAPLSWRFHLALASNTEDNTAVQDPTLTGLYSKVKKSTKRPFSLPSSTLEDPLKVED
Notophthalums viridescens    SSIPAHVSWRFHLAPAPNTEDSTTAEDQRLKGLYSKVKKNAKHP----------------
Pleurodeles waltl            TSTPP-LLWRFHLSLASNTEDKTTAQDPILKDLYSKVKKNPKRPDSLLSSTVEHPIKVED
Ambystoma mexicanum          TPDHTVLSWRFHLSLAADEEGSTEAQNPERNALYTKIK-HTKDIAPFPSPTSETPPEDDN
                             :.  . : *****: *.: *..* .::   . **:*:*  .*

Cynops pyrrhogaster          DVPPPVPVKQFDIEED---LSTQNQDIEDPLPPPPILLIN
Notophthalums viridescens    ----------------------------------------
Pleurodeles waltl            DVPPPVPIKRFNVEED---LFTQNQDIEEPLPLPPILGIN
Ambystoma mexicanum          DMPPPVPKKRFNIEEEQFHLQSNNQDTEEPLPPPPILEIN
```

B

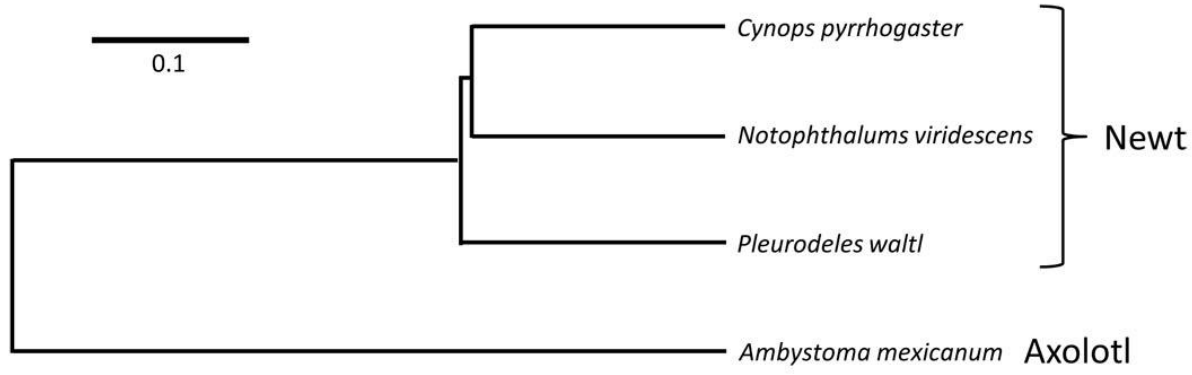

Fig 8. Comparison of Newtic1 protein among urodele species.

A) Multiple alignment by ClustalW among *C. pyrrhogaster*, *N. viridescens*, *P. waltl* and *A. mexicanum*. TM indicates the transmembrane domain predicted by InterProScan (https://www.ebi.ac.uk/interpro/search/sequence-search). **(B)** Phylogenetic relationships constructed by neighbor-joining method, comparing contigs of *Notophthalmus viridescens*, *Pleurodeles waltl* and *Ambystoma mexicanum* (image adapted from Casco et. al, 2018).

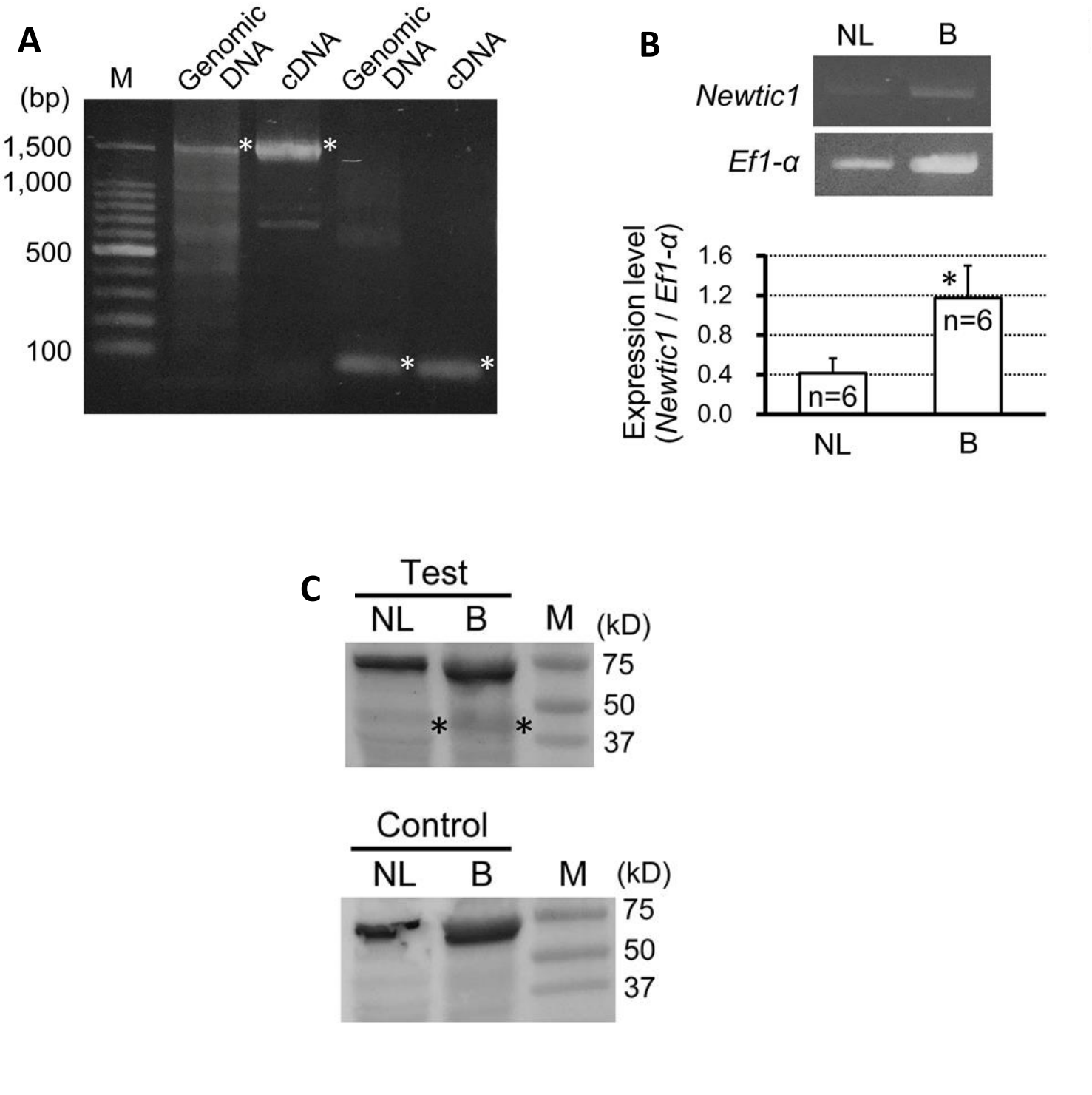
A
M
Genomic DNA
cDNA
Genomic DNA
cDNA
(bp)
1,500
1,000
500
100
*
*
*
*
B
NL
B
Newtic1
Ef1-α
Expression level (Newtic1 / Ef1-α)
1.6
1.2
0.8
0.4
0.0
n=6
n=6
*
NL
B
C
Test
NL
B
M
(kD)
75
50
37
*
*
Control
NL
B
M
(kD)
75
50
37

Fig. 9 PCR and Immunoblotting results of Newtic1.

(A) Molecular cloning of Newtic1 evaluating 2 amplicon sizes. Genomic DNA of blood, and cDNA of the blastema were used as a template. Asterisk indicate the designated band. **(B)** Semi-quantitative analysis was performed showing the expression levels of Newtic1 in NL and B. Samples were amplified by PCR with NL and B cDNA samples (n = 6 each). Ef1-α was also amplified as an internal control. The quantity of the PCR product of Newtic1 was normalized to Ef1-α in the same cDNA sample. The mean expression level of Newtic1 in B was significantly higher than that in NL (Student's t-test, *$p < 0.05$). it must be noted that weak Newtic1 expression was detected, as shown in 4 of 6 NL samples. **(C)** Presence of Newtic1 protein. Western blot was carried out with the same volume of protein samples which were extracted from the same weight of NL and B samples (n = 3). The NL and B protein samples were blotted on the same membrane. Using Newtic1 antibody (Test), weak protein bands corresponding to Newtic1 (40.7 kD) were detected in both samples (asterisks), although the band intensity in the blastema was slightly higher. For the control, Newtic1 antibody was replaced with RFP antibody. The membranes for Test and Control were stained separately. The 60–70 kD bands were caused by a non-specific reaction of the secondary antibody. M: marker; (adapted from Casco et. al, 2018).

A

Newtic1 Nuclei vim

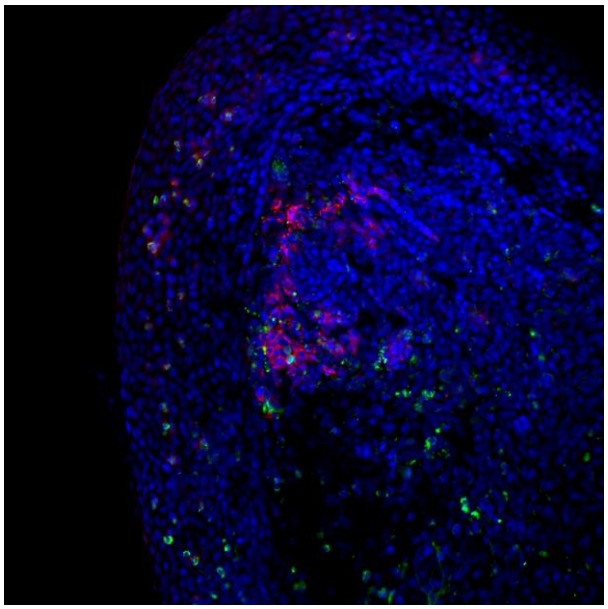

B

Newtic1 Nuclei vim

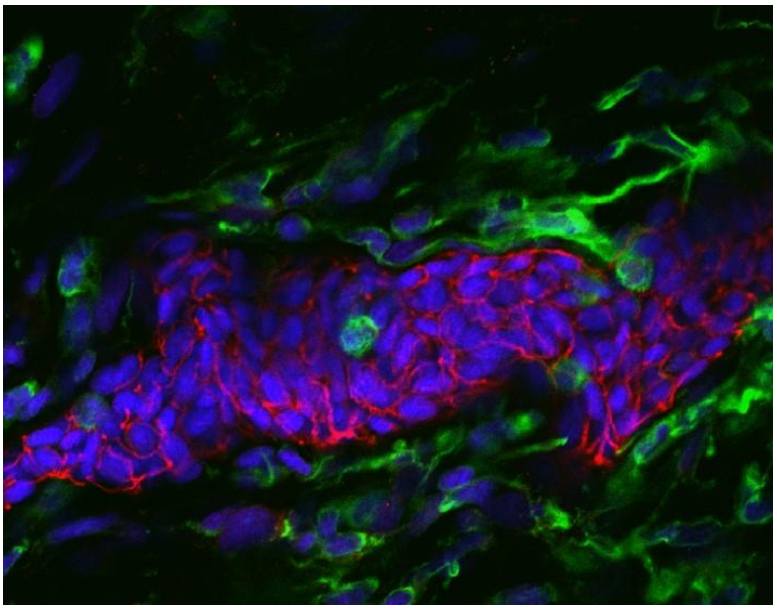

Fig. 10 Preliminary Observation of Newtic1 within blastema tissue and blood vessels.

(A) Blastema at 27DPA – stage III – MB showing red immunoreactivity to cells within the distal blastema. **(B)** Blood vessel displaying with Newtic1 positive cells within the radial blood vessel of an intact limb sample (image adapted from Casco et. al, 2018).

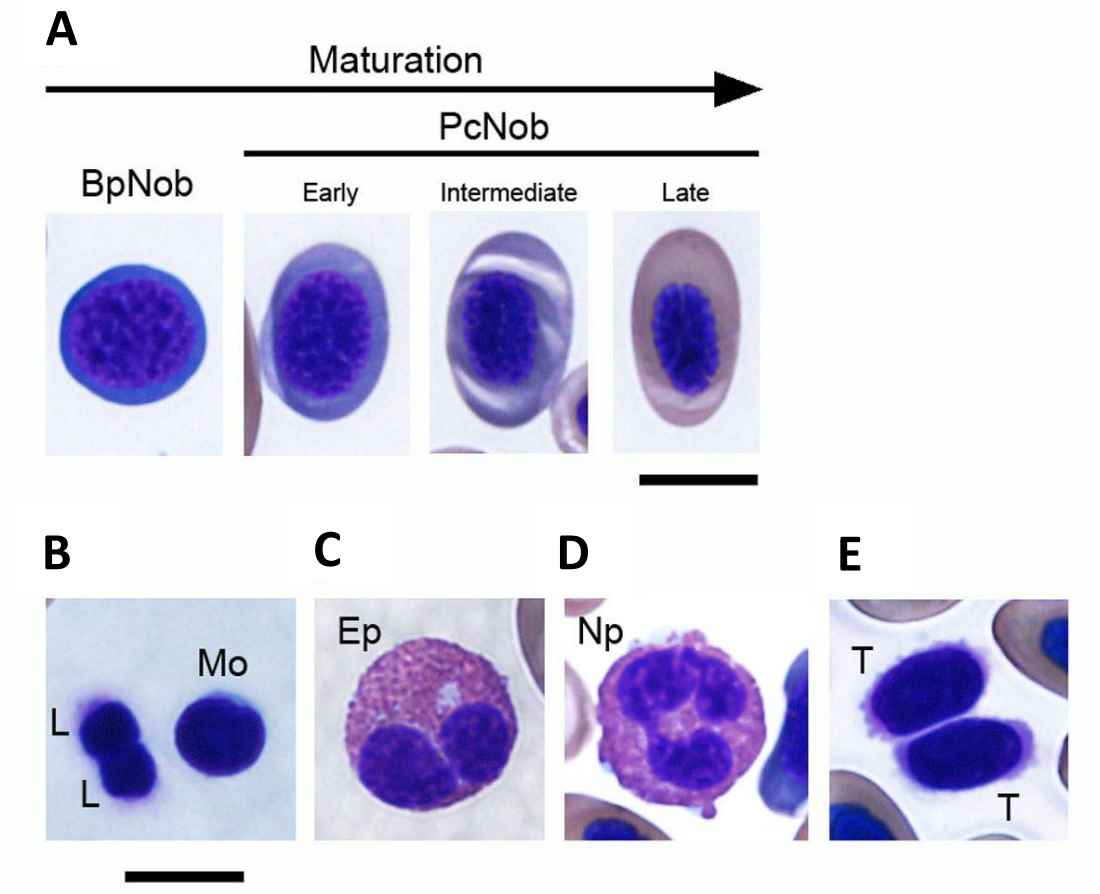
A
Maturation
PcNob
BpNob
Early
Intermediate
Late
B
C
D
E
Mo
L
L
Ep
Np
T
T

Fig 11. Cataloging Erythrocytes with Wright-Giemsa stain.

Peripheral blood was obtained from adult animals by amputating their forearms. **(A)** Nucleated erythrocytes (normoblasts) at different developmental stages. Normoblasts were divided into basophilic normoblasts (BpNobs) and polychromatic normoblasts (PcNobs). BpNobs are an immature state of normoblasts, which are characterized by their oblate spheroid shape with a big round polychromatic nucleus and a narrow cytoplasmic space. The cytoplasm is stained in blue. PcNobs are defined as normoblasts in a transitional to mature state. In this study, PcNobs cells were subdivided into early, intermediate and late stages: PcNobs at intermediate and late stages, which looked similar in morphology, were grey and pink/orange in color with the cytoplasmic stain, respectively; PcNobs at an early stage had a larger and rounder nucleus, and had less cytoplasmic space that was stained blue. Other cell types were also observed in much smaller quantities than PcNob proportions: **(B)** Monocytes (Mo) and lymphocytes (L). **(C)** Eosinophil (Ep). **(D)** Neutrophil (Np). **(E)** Thrombocytes (T). Scale bar, 20 μm (image adapted from Casco et. al, 2018).

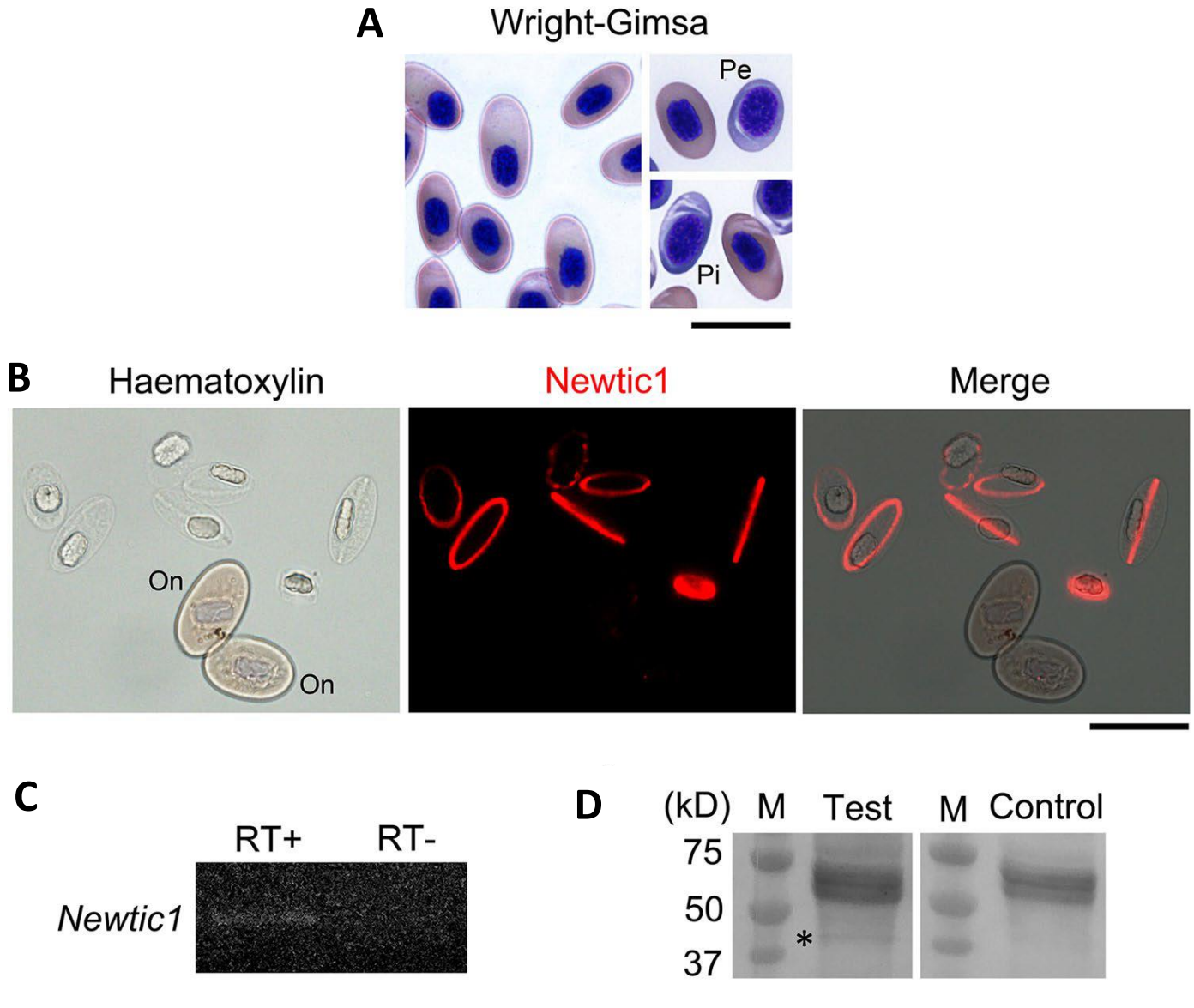
A
Wright-Gimsa
Pe
Pi
B
Haematoxylin
Newtic1
Merge
On
On
C
RT+
RT-
Newtic1
D
(kD)
M
Test
M
Control
75
50
37
*

Fig 12. Newtic1 is specifically expressed in a subset of erythrocytes.

(A) Adult newt erythrocytes. Wright-Giemsa stain of blood (peripheral blood) revealed a large number of nucleated erythrocytes (normoblasts) (n = 10). Most of them (~99%) were polychromatic normoblasts (PcNobs) at different developmental stages. Scale bar, 40 μm. **(B)** Newtic1 immunoreactivity in blood cell suspensions (n = 9). Under this set of experimental conditions, almost all PcNobs became slightly swollen and transparent. Newtic1 immunoreactivity was exclusively observed along the equator of those PcNobs. Nuclei were lightly stained with haematoxylin. On: presumptive orthochromatic normoblasts; Scale bar, 40 μm. **(C)** Confirmation of the presence of Newtic1 transcripts in blood cells (n = 3). Total RNA was purified from whole blood cells (proportion of normoblasts was estimated 83–94%). The 497 bp sequence of Newtic1 was amplified by RT-PCR (RT+), but not without reverse transcription (RT−). Products were electrophoresized on the same gel. **(D)** Confirmation of the presence of Newtic1 protein in blood cells (n = 3). Western blotting was carried out with protein samples purified from whole blood cells. Newtic1 antibody (Test) labeled a band corresponding to Newtic1 protein (40.7 kD; asterisk), while RFP antibody (Control) did not. The membranes for Test and Control were stained separately. The 60–70 kD bands were caused by a non-specific reaction of the secondary antibody. M: marker (image adapted from Casco et. al, 2018).

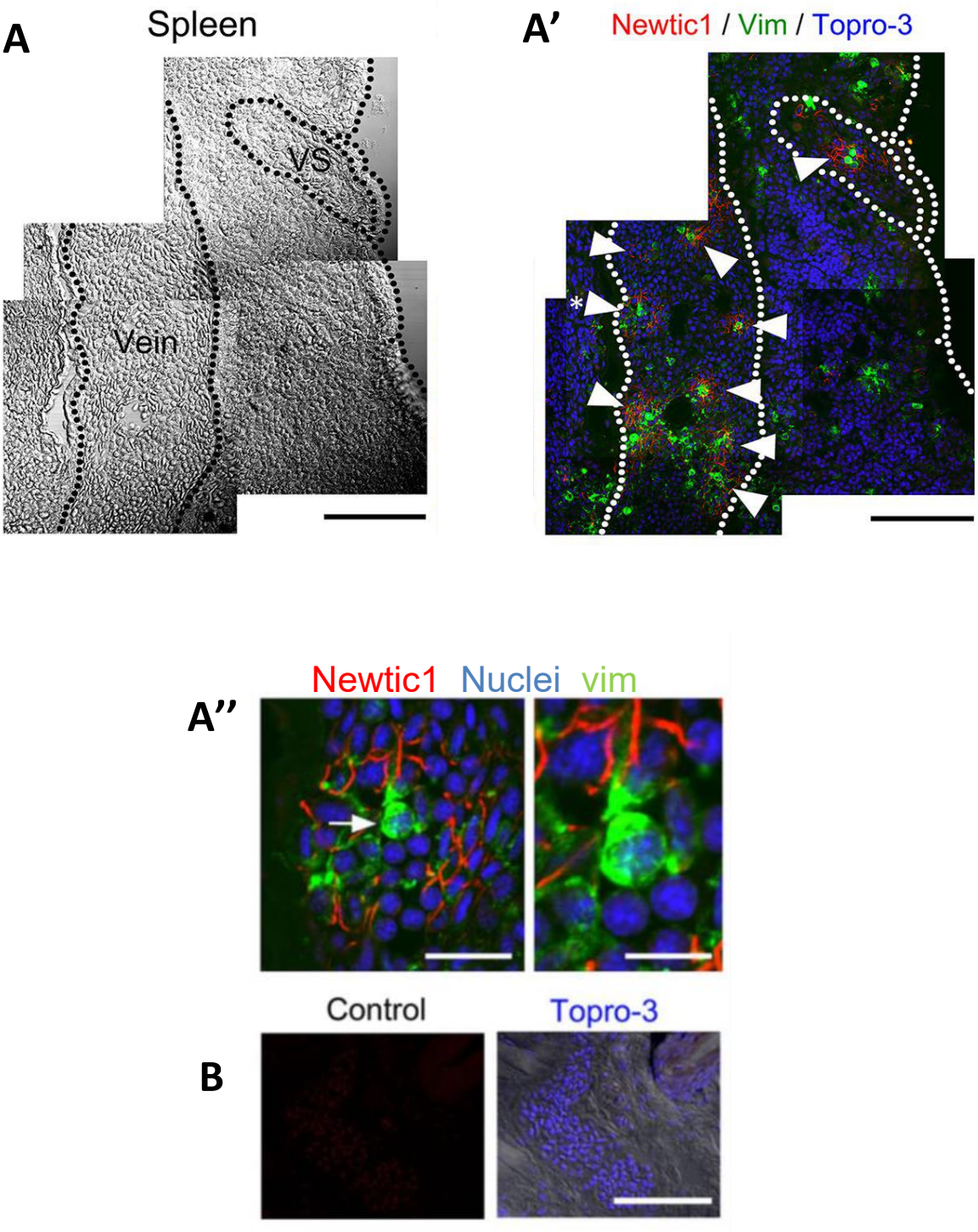
A
Spleen
VS
Vein
A'
Newtic1 / Vim / Topro-3
*
A''
Newtic1 Nuclei vim
B
Control
Topro-3

Fig 13. Newtic1-expressing erythrocytes form an aggregate structure EryC, which is accompanied by monocytes and circulating throughout the Spleen.

(A-B) Representative images showing EryCs in the spleen (n = 3). **(A)** A section of the spleen. VS: Venus sinus. Scale bar, 200 μm. **(A′)** Immunofluorescence labeling of the same section with Newtic1 antibody (red) and vimentin antibody (green). Arrowheads point to EryCs.Topro-3: nucleus. Scale bar, 200 μm. **(A′′)** Enlargement of EryCs (asterisk in A′). EryCs were accompanied by spherical cells with vimentin-immunoreactivity (arrow). Scale bar, 40 μm. Enlargement of a spherical cell (arrow in A′′). Scale bar, 40 μm. **(B)** Negative control for the immunofluorescence labeling of blood-containing vessels (n = 3). Control: labeling with RFP antibody (red). Topro-3: nucleus. Scale bar, 200 μm (image adapted from Casco et. al, 2018).

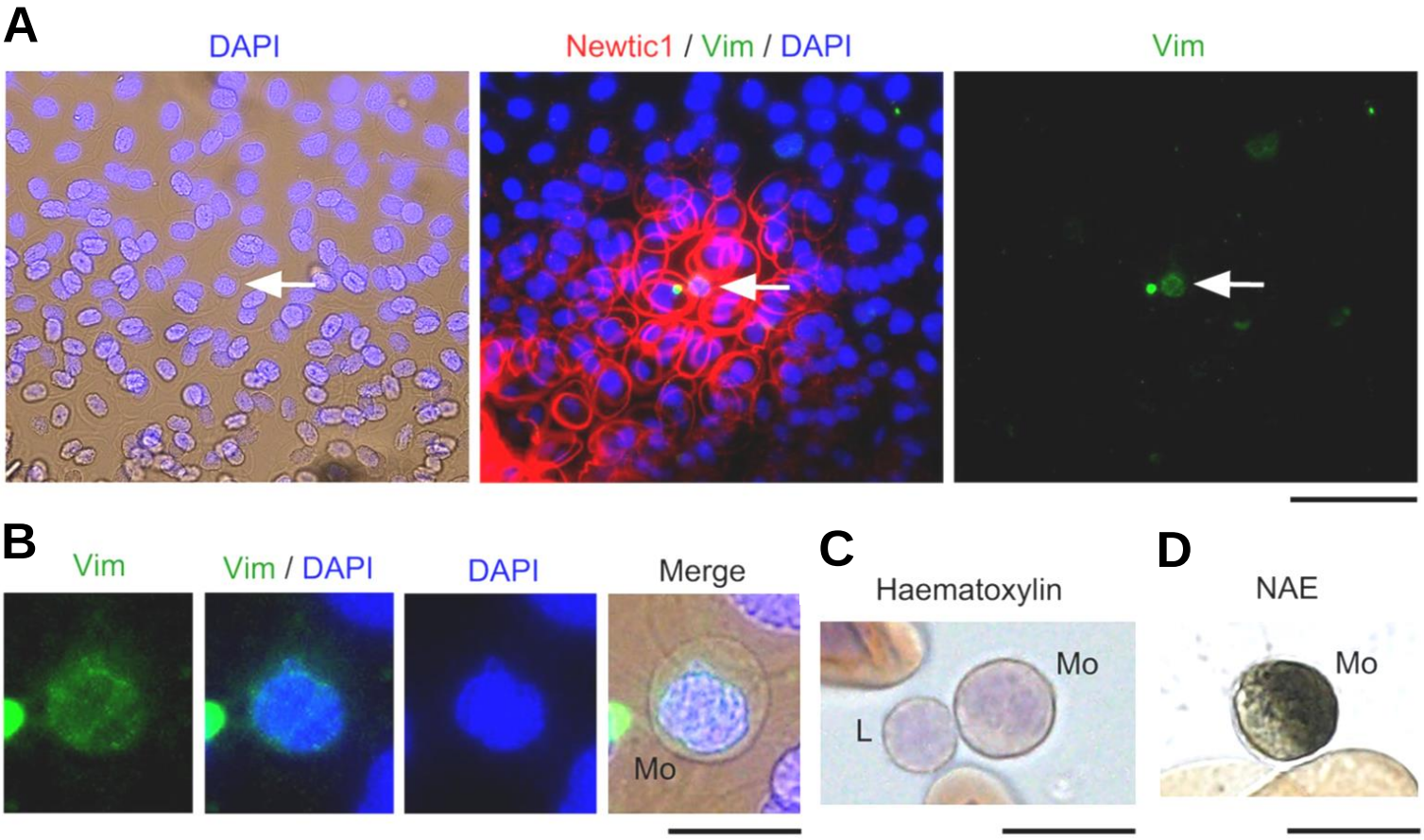
A
DAPI
Newtic1 / Vim / DAPI
Vim
B
Vim
Vim / DAPI
DAPI
Merge
Mo
C
Haematoxylin
Mo
L
D
NAE
Mo

Fig 14. Immunofluorescence labeling of blood cell smears with Newtic1 and vimentin antibodies.

Newtic1 antibody (red) and vimentin antibody (green). **(A)** Peripheral blood was collected in a plastic dish and allowed to coagulate to preserve the structure of EryCs. Newtic1-immunoreactivity was only observed in PcNobs of EryCs, but not in free PcNobs scattered around EryCs. Arrow: Vim+ cell. DAPI: nucleus. Scale bar, 80 μm. **(B)** Enlargement of the Vim+ cell (arrow in A). Vim+ cells were 16–20 μm in diameter and had a brain-shaped nucleus surrounded by vimentin. From these morphological characteristics, Vim+ cells were identified as monocytes (Mo) Note that Vim+ cells in blood were always monocytes. Scale bar, 20 μm**. (C)** Representative image of hematoxylin stain of the adult newt monocyte (Mo) and lymphocyte (L). Scale bar, 20 μm. **(D)** Example image of adult newt monocytes identified by α-naphthyl acetate esterase (NAE) activity in their cytoplasm. Scale bar, 20 μm (image adapted from Casco et. al, 2018).

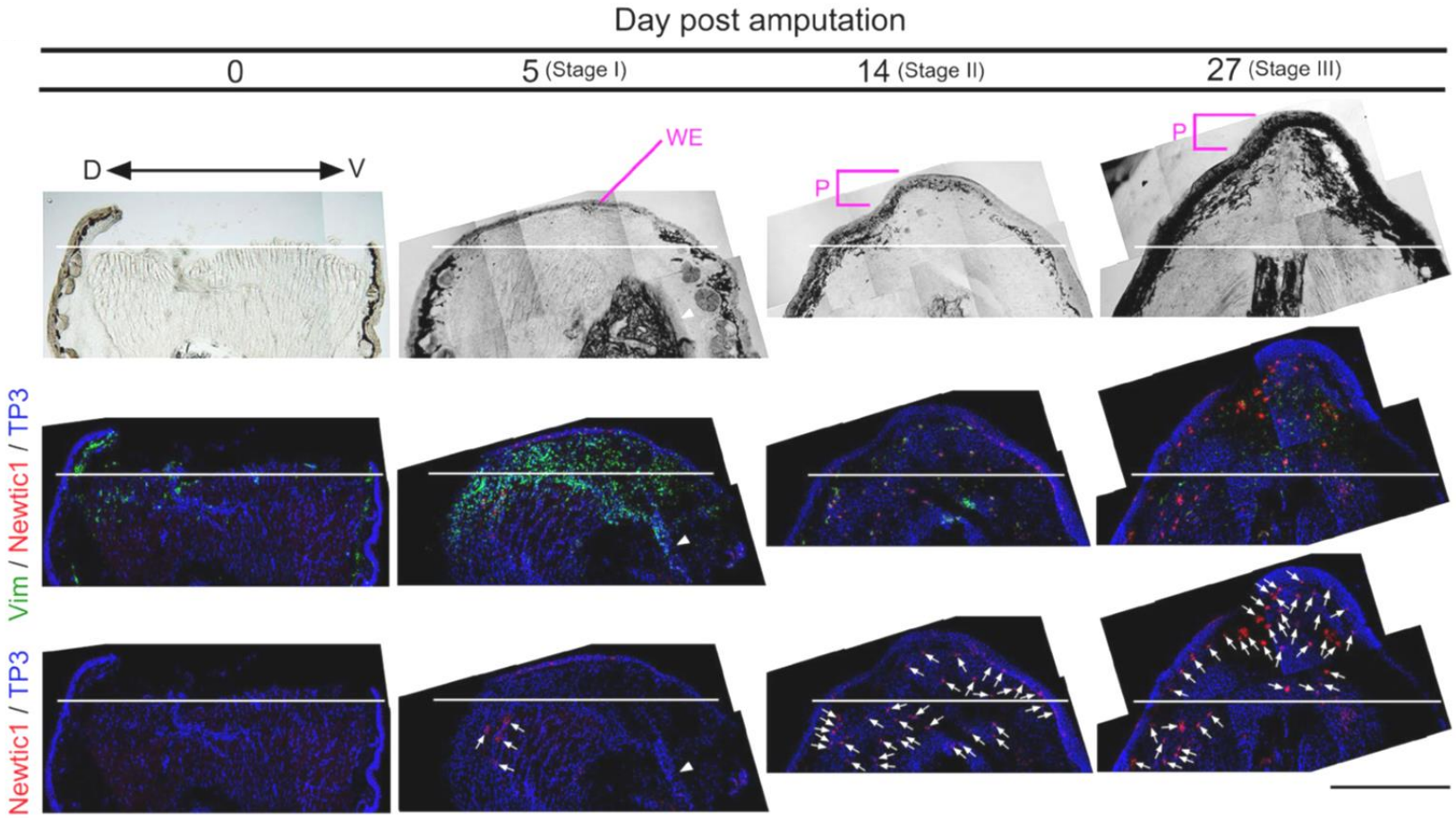
Day post amputation
0
5 (Stage I)
14 (Stage II)
27 (Stage III)
D
V
WE
P
P
Vim / Newtic1 / TP3
Newtic1 / TP3

Fig. 15 EryCs are newly generated in the limb stump and accumulated in a distal portion of the blastema.

(A) Change in distribution pattern of EryCs and vimentin-immunoreactive (Vim+) cells during blastema formation (n = 4 each). Arrows indicate EryCs. Arrowheads in 5 DPA indicate a large blood vessel containing Vim+ cells. Key stages are depicted in the early regenerative process: 0 DPA, immediately after amputation – Almost no EryCs can be observed at the amputation site; 5 DPA – Stage I displays a large quantity of Vim+ cells accumulating at the distal stump; 14 DPA – Stage II displays an emerging protrusion of the blastema with EryCs beginning to from and accumulate in the proximal region; and 27 DPA – stage III displays EryCs have accumulated at the Distal region of the Protrusion. White line indicates the amputation plane. WE: wound epidermis. P: protrusion. Topro-3 (TP3): nucleus. D: dorsal side. V: ventral side. Scale bar, 1 mm (image adapted from Casco et. al, 2018).

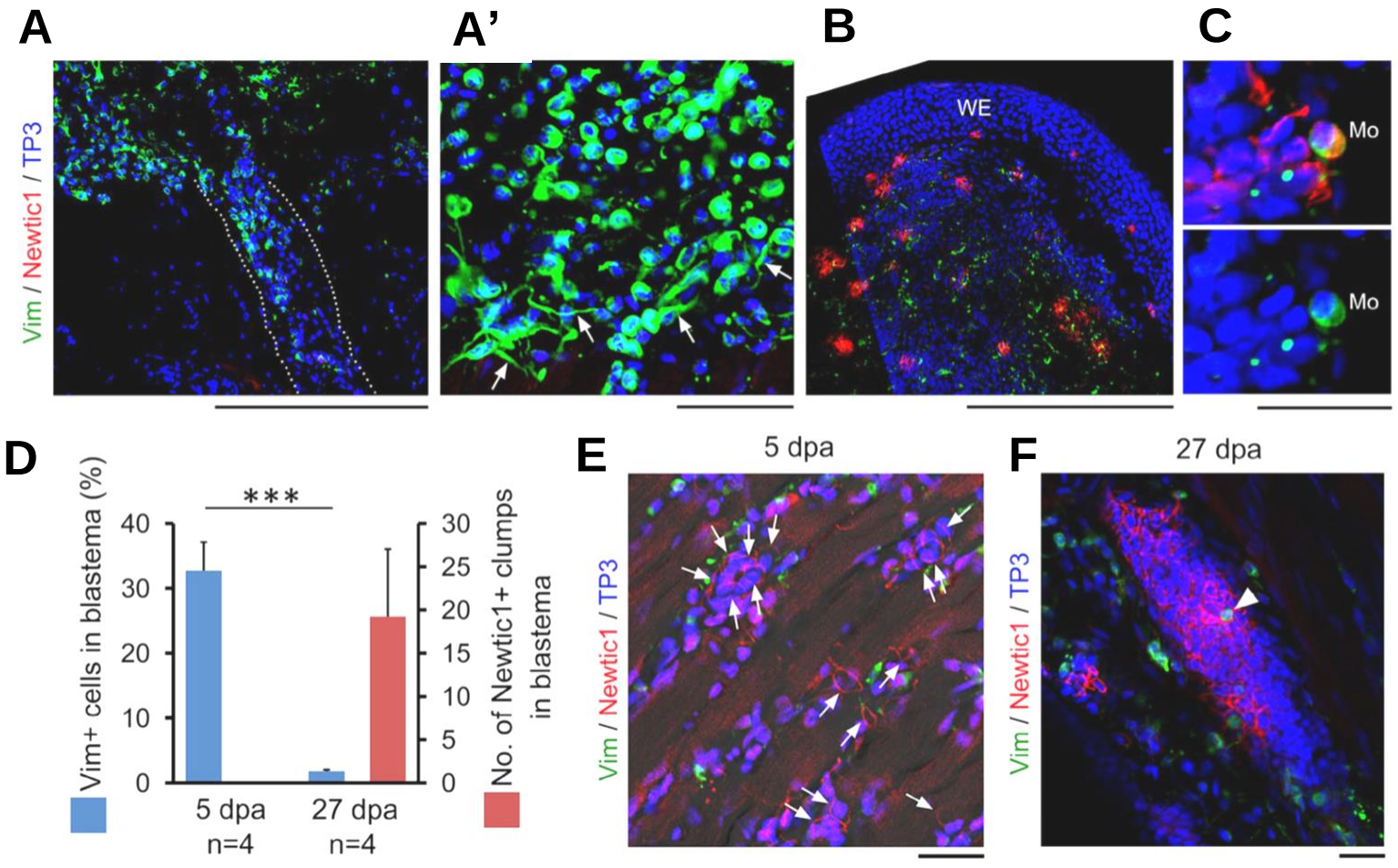
A
A'
B
C
Vim / Newtic1 / TP3
WE
Mo
Mo
D
E
F
5 dpa
27 dpa
***
Vim+ cells in blastema (%)
No. of Newtic1+ clumps in blastema
40
30
20
10
0
30
25
20
15
10
5
0
5 dpa
n=4
27 dpa
n=4
Vim / Newtic1 / TP3
Vim / Newtic1 / TP3

Fig. 16 EryCs are newly generated in the limb stump and accumulated in a distal portion of the blastema.

(A) Enlargement of the blood vessel (arrowhead in Fig. 15 –Stage III). Dotted lines indicate the wall of the vessel. Vim+ cells in the vessel, which were exclusively monocytes, seemed to be released from the opening of the vessel into the blastema. Scale bar, 500 μm. **(A′)** Enlargement of Vim+ cells in the blastema at 5 DPA in (Fig 15 – stage I). Almost all of the Vim+ cells were morphologically identified as monocytes. Some cells with long processes (arrows) that gathered around the amputation plane also showed vimentin immunoreactivity. Scale bar, 100 μm. **(B)** Enlargement of the protrusion of blastema at 27 DPA – stage III in (Fig. 15). Scale bar, 500 μm. **(C)** Representative image showing monocytes (Mo) in the blastema at 27 DPA (n = 3). Scale bar, 50 μm. **(D)** The proportion of Vim+ cells and the number of Newtic1+ clumps in a blastema at 5 and 27 DPA. At 5 DPA, Vim+ cells (178-283/section) occupied ~32.8% of cells in the blastema, while Newtic1 immunoreactivity did not appear in the blastema. In contrast, at 27 DPA, a large number of Newtic1+ clumps were distributed in the blastema (11–32/section), while the proportion of Vim+ cells in the blastema (7–17/section) declined to ~1.8% (Welch's t-test, ***$p < 0.001$; see Methods). **(E)** Appearance of Newtic1 immunoreactivity in PcNobs accumulated in dilated capillaries in the region proximal to the amputation plane at 5 DPA. Red signal was enhanced in the image at 5 DPA to reveal weak fluorescence of Newtic1 immunoreactivity. Arrows point to Newtic1-immunoreactive PcNobs in dilated capillaries in between muscle fibers. Scale bar, 50 μm. **(F)** Accumulation of Newtic1-immunoreactive PcNobs in thick blood vessels in the region proximal to the amputation plane in the regenerating forearm at 27 DPA (n = 3). Monocytes were occasionally observed in the blood stream (arrowhead). Scale bar, 100 μm (image adapted from Casco et. al, 2018).

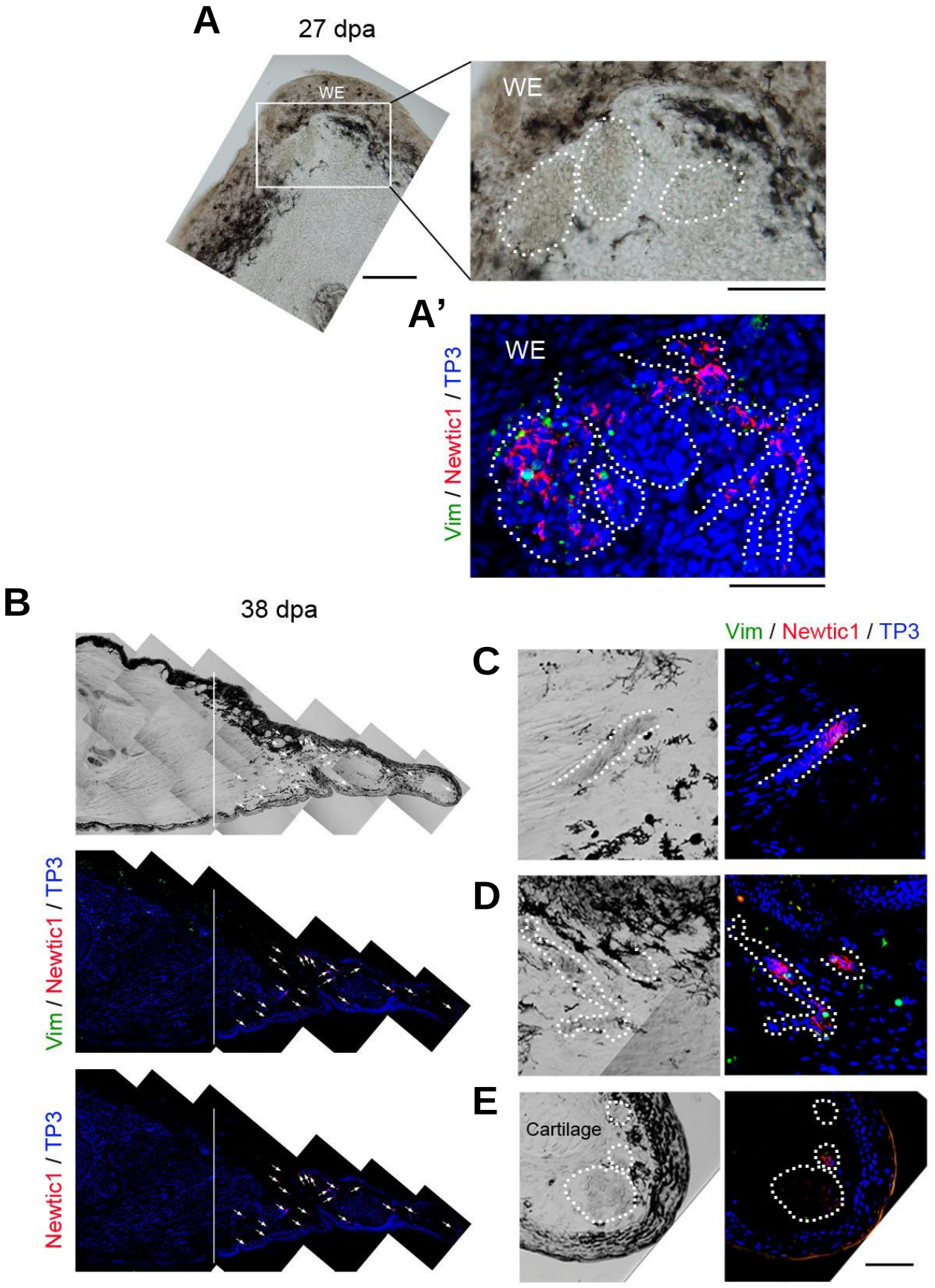
A
27 dpa
WE
WE
A'
WE
Vim / Newtic1 / TP3
B
38 dpa
Vim / Newtic1 / TP3
Vim / Newtic1 / TP3
C
D
E
Cartilage
Newtic1 / TP3

Fig. 17 EryCs are transported through regenerating capillaries/vessels.

(A, A′) A section showing thick blood vessels (dotted lines) in the protrusion of the blastema at 27 DPA. WE: wound epidermis. Scale bars, 300 μm (left) and 200 μm (right). **(A′)** A section showing the presence of EryCs in regenerating capillaries/vessels (dotted lines) in the protrusion of the blastema at 27 DPA. Regenerating capillaries/vessels formed the loops (or network) with large ventricles, in which EryCs accumulated to form larger Newtic1+ aggregates. Scale bar, 100 μm. **(B)** Representative image showing the distribution pattern of EryCs (arrows) in a regenerating forearm at 38 DPA (n=3). Vertical line: amputation plane. EryCs were mostly distributed within the regenerate, although the size and density of Newtic1+ aggregates decreased compared to those in the blastema at stage III (Fig. 15 stage III). Immunoreactivity of the region proximal to the amputation plane recovered as in an intact limb. Scale bar, 1 mm. **(C-E)** Enlargement of EryCs in B. EryCs seemed to be flowing along blood capillaries/vessels (dotted lines). Note that EryCs at this stage were always accompanied by monocytes as observed in normal blood (Fig. 10 and Splenic tissue samples; Fig. 12). Scale bar, 100 μm (image adapted from Casco et. al, 2018).

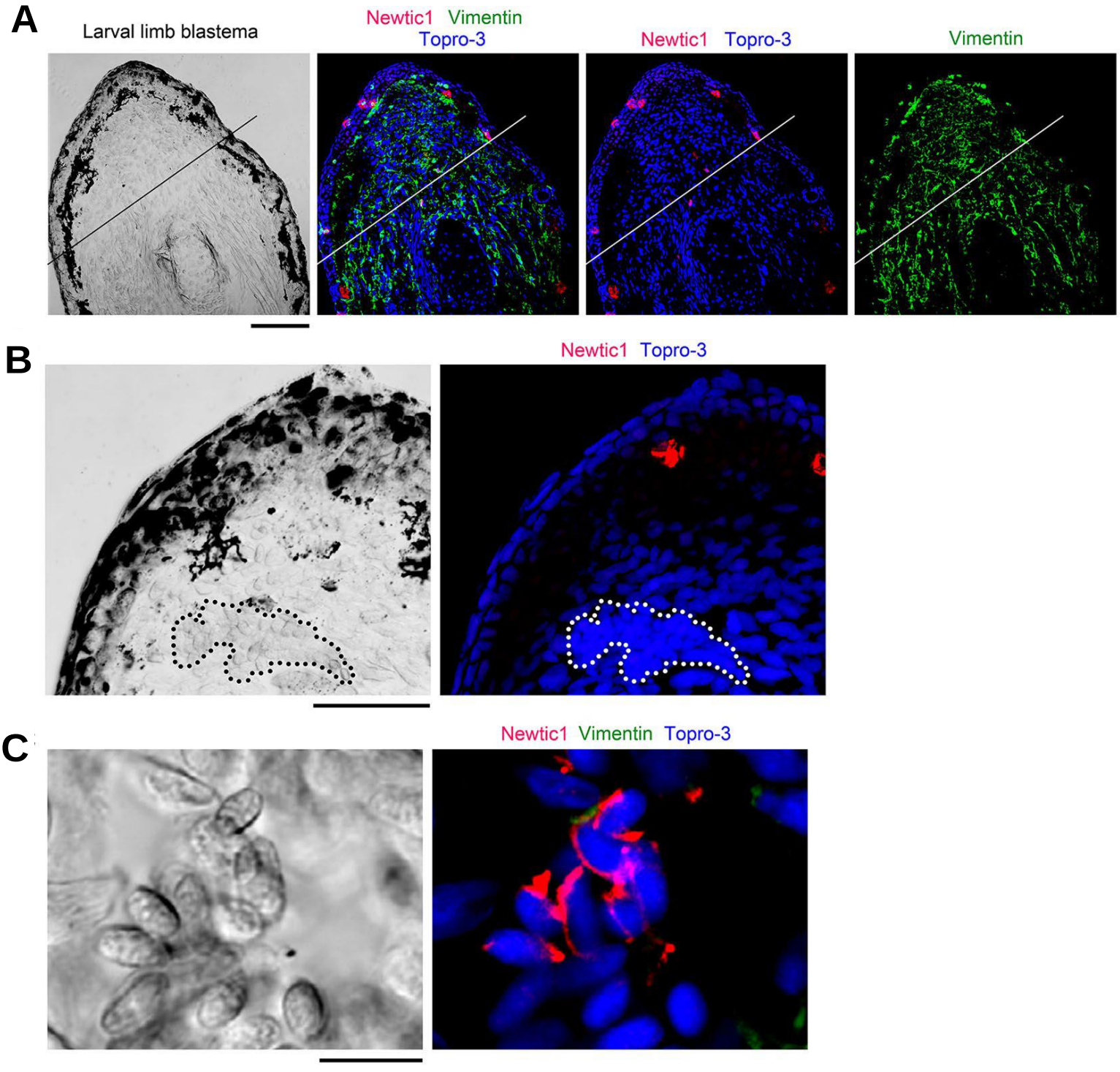
A
Larval limb blastema
Newtic1 Vimentin
Topro-3
Newtic1 Topro-3
Vimentin
B
Newtic1 Topro-3
C
Newtic1 Vimentin Topro-3

Fig. 18. Newtic1-expressing erythrocytes do not contribute to larval limb blastema.

(A) Representative image showing immunoreactivity in the blastema of the forearm in swimming larvae ~3 months old (stage 57–58; n = 3). Line: amputation plane. In contrast to adult limbs, Newtic1 immunoreactivity was hardly observed in mesenchymal cells in the blastema, while a large number of fibrous cells were labeled with Vimentin antibody. It is important to note that in larval limbs, Newtic1 displayed immunoreactivity to gland-like structures along the wound epidermis and Vimentin antibody labeled many fibrous cells similar to fibroblasts. Topro-3 (TP3): nucleus. Scale bar, 200 μm. **(B)** A section showing a large blood vessel (dotted line) in the blastema. No Newtic1+ cells were present in blood capillaries/vessels in the blastema (n = 3). Scale bar, 100 μm. **(C)** Newtic1+ erythrocytes in swimming larvae ~3 months old (stage 57–58). Larval erythrocytes (longer axis: ~15 μm) were about half the size of those from adults. Newtic1+ showed immunoreactivity to erythrocytes but was rarely observed (2 of 26 sections from 9 limbs). These cells were not associated with either Vim+ cells or cells such as monocytes. Scale bar, 100 μm (image adapted from Casco et. al, 2018).

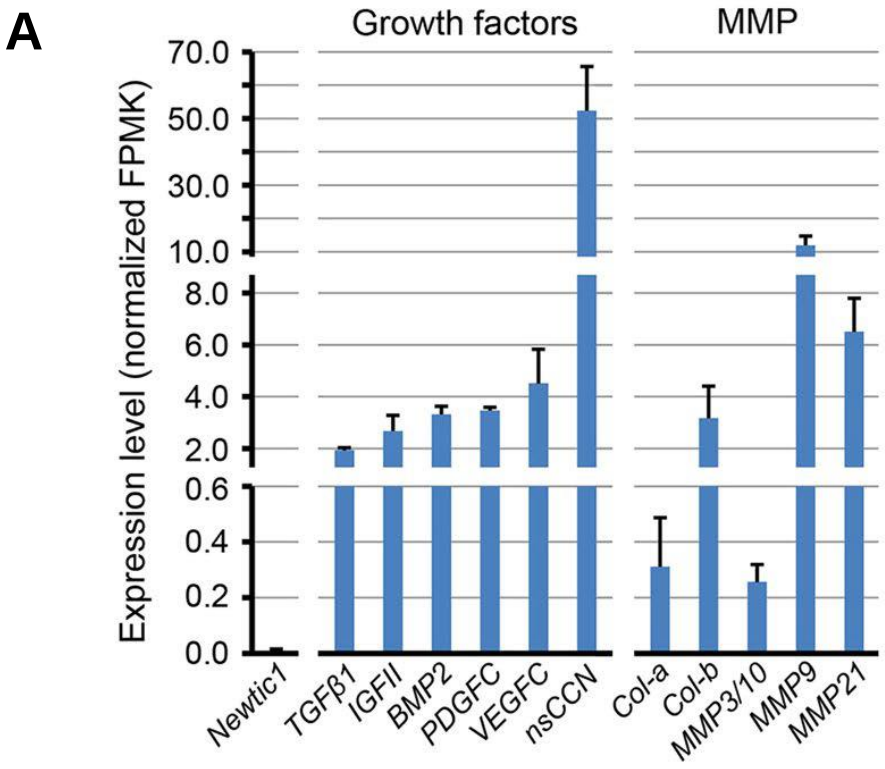
A
Growth factors
MMP
Expression level (normalized FPMK)
70.0
50.0
30.0
10.0
8.0
6.0
4.0
2.0
0.6
0.4
0.2
0.0
Newtic1
TGFβ1
IGFII
BMP2
PDGFC
VEGFC
nsCCN
Col-a
Col-b
MMP3/10
MMP9
MMP21

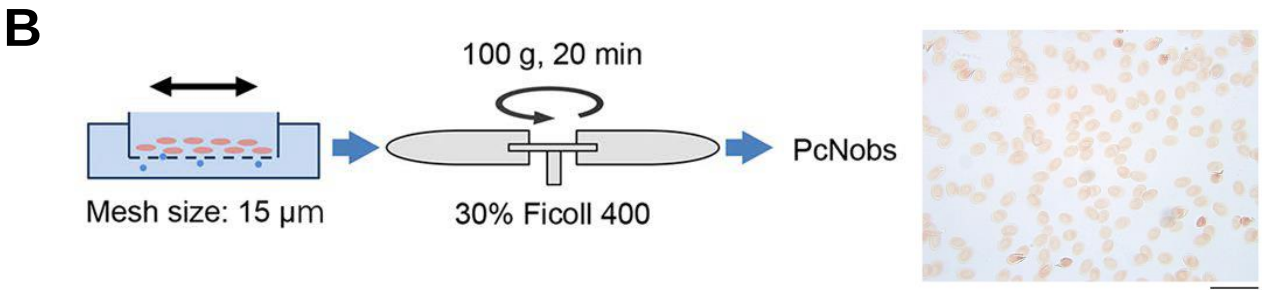
B
100 g, 20 min
PcNobs
Mesh size: 15 μm
30% Ficoll 400

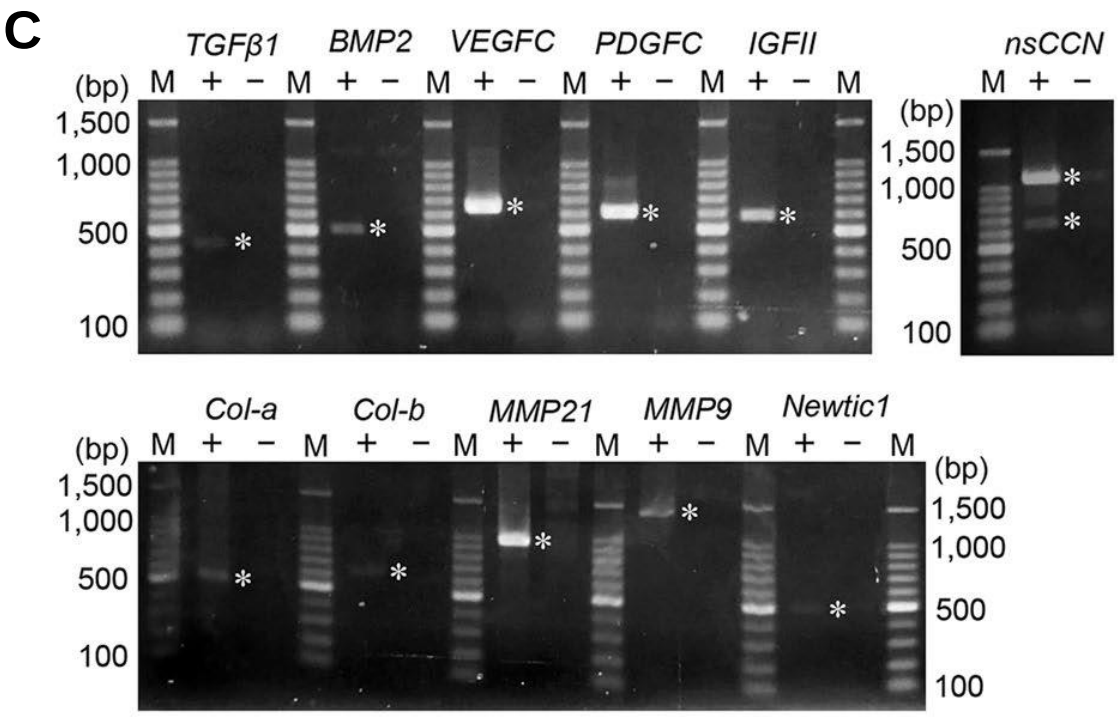
C
TGFβ1
BMP2
VEGFC
PDGFC
IGFII
nsCCN
(bp)
M + − M + − M + − M + − M + − M
1,500
1,000
500
100
M + −
Col-a
Col-b
MMP21
MMP9
Newtic1

Fig. 19. Circulating erythrocytes express genes of a large number of secretory molecules.

(A) Relative gene expression levels of secretory molecules (growth factors and MMPs) as well as Newtic1 in whole blood. mRNA-seq was carried out (n = 3) and aligned the sequence reads on TOTAL. **(B)** Isolation of red blood cells using a filter/centrifuge system leading to purified collection of red blood cells. **(C)** PCR confirmation of gene expression in PcNobs (n = 3). PcNobs were purified (99.3–99.8%) from whole blood through a sieve and isopynic centrifugation. The representative data set shown here was obtained with the same cDNA sample (+) and its original RNA sample without reverse transcription (−). PCR products (+ and −) of growth factors, those of MMPs and Newtic1, and that of nsCCN were electrophoresized on the same gel each. The transcription of all of the genes listed in **(A)** were detected (asterisk). As for nsCCN, two bands corresponding to the variants were detected. M: marker.

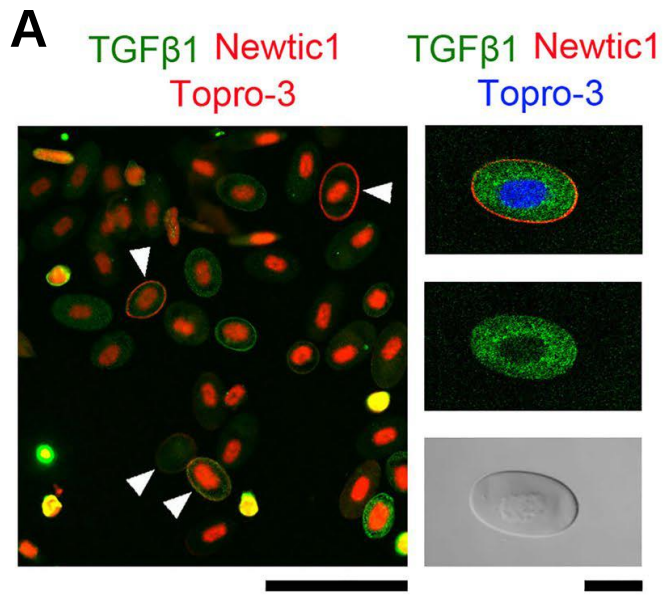
A
TGFβ1 Newtic1
Topro-3
TGFβ1 Newtic1
Topro-3

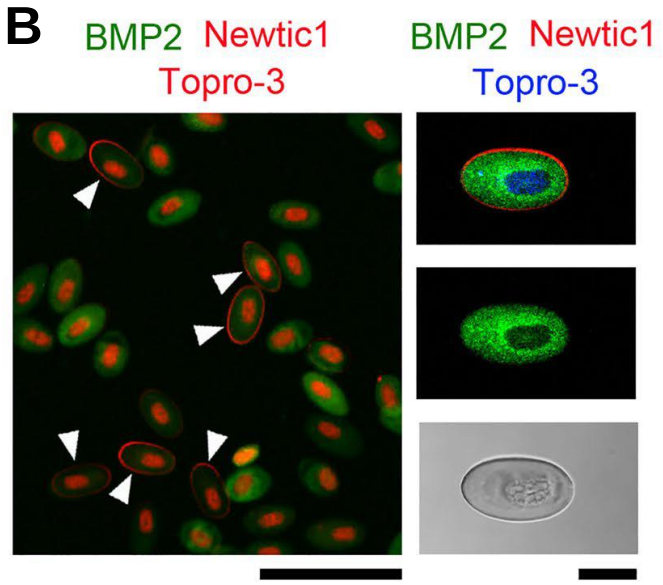
B
BMP2 Newtic1
Topro-3
BMP2 Newtic1
Topro-3

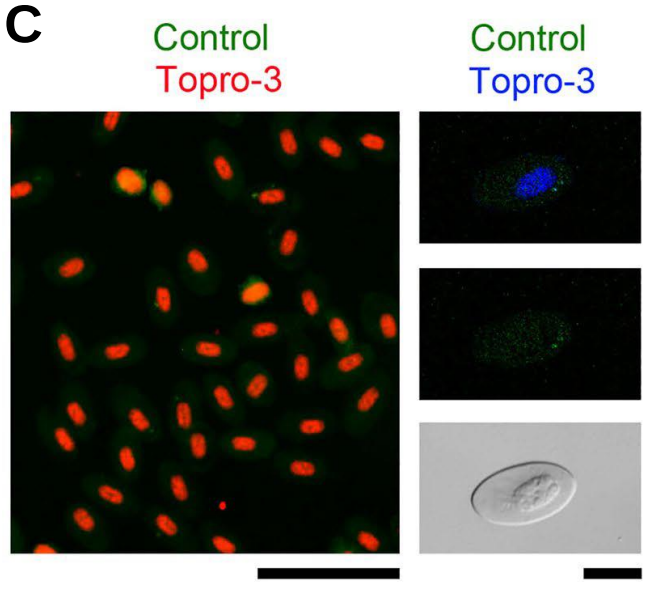
C
Control
Topro-3
Control
Topro-3

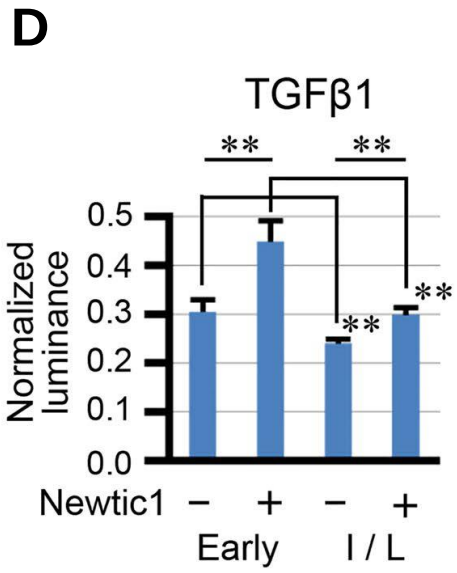
D
TGFβ1
Normalized luminance
0.0
0.1
0.2
0.3
0.4
0.5
**
**
**
**
Newtic1 − + − +
Early I / L

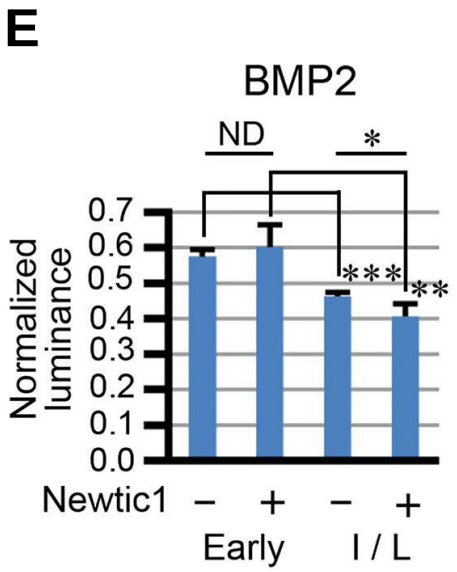
E
BMP2
ND
*
***
**
Normalized luminance
0.0
0.1
0.2
0.3
0.4
0.5
0.6
0.7
Newtic1 − + − +
Early I / L

Fig. 20 TGFβ-1 and BMP2 are expressed in circulating erythrocytes.

(A) Representative image showing TGFβ-1 expression in PcNobs (n = 6). PcNobs in blood cell suspensions were double labeled with TGFβ-1 (green) and Newtic1 (red) antibodies. Nuclei were also labeled with Topro-3 (blue). Arrowheads point to Newtic1-positive (Newtic1+) PcNobs. PcNobs exhibited TGFβ-1 immunoreactivity but their fluorescence intensity was variable. Note that the fluorescence intensity was sometimes higher along the equator of PcNobs, independent of the intensity of Newtic1 immunoreactivity. Scale bar, 100 μm. Right hand column shows a particular Newtic1+ PcNob exhibiting intense TGFβ-1 immunoreactivity in its cytoplasm. Upper two panels show confocal images. Scale bar, 20 μm. **(B)** Representative image showing BMP2 expression in PcNobs (n = 3). PcNobs in blood cell suspensions were double labeled with BMP2 (green) and Newtic1 (red) antibodies. The data are presented in the same manner as in (A). PcNobs exhibited BMP2 immunoreactivity, but as in TGFβ-1, their fluorescence intensity varied. **(C)** Control immunoreactivity (n = 3). PcNobs in blood cell suspensions were labeled with control (RFP; green) antibody. The data are presented in the same manner as in (A). **(D)** Relationships of TGFβ-1 expression in PcNobs with either their developmental stage or Newtic1 expression. Representative images obtained from six experiments in (A) were used. Total number of PcNobs at an early stage: Newtic1−, n = 51; Newtic1+, n = 41. Total number of PcNobs at an intermediate/ late stage: Newtic1−, n = 255; Newtic1+, n = 110. **(E)** Relationships of BMP2 expression in PcNobs with either their developmental stage or Newtic1 expression. Representative images obtained from three experiments in (B) were used. Total number of PcNobs at an early stage: Newtic1-, n = 74; Newtic1+, n = 11. Total number of PcNobs at an intermediate/late stage: Newtic1−, n = 231; Newtic1+, n = 30. Statistical difference: Student's t-test/Welch's t-test; *p < 0.05, **p < 0.01, ***p < 0.001, ND (no difference) (image adapted from Casco et. al, 2018).

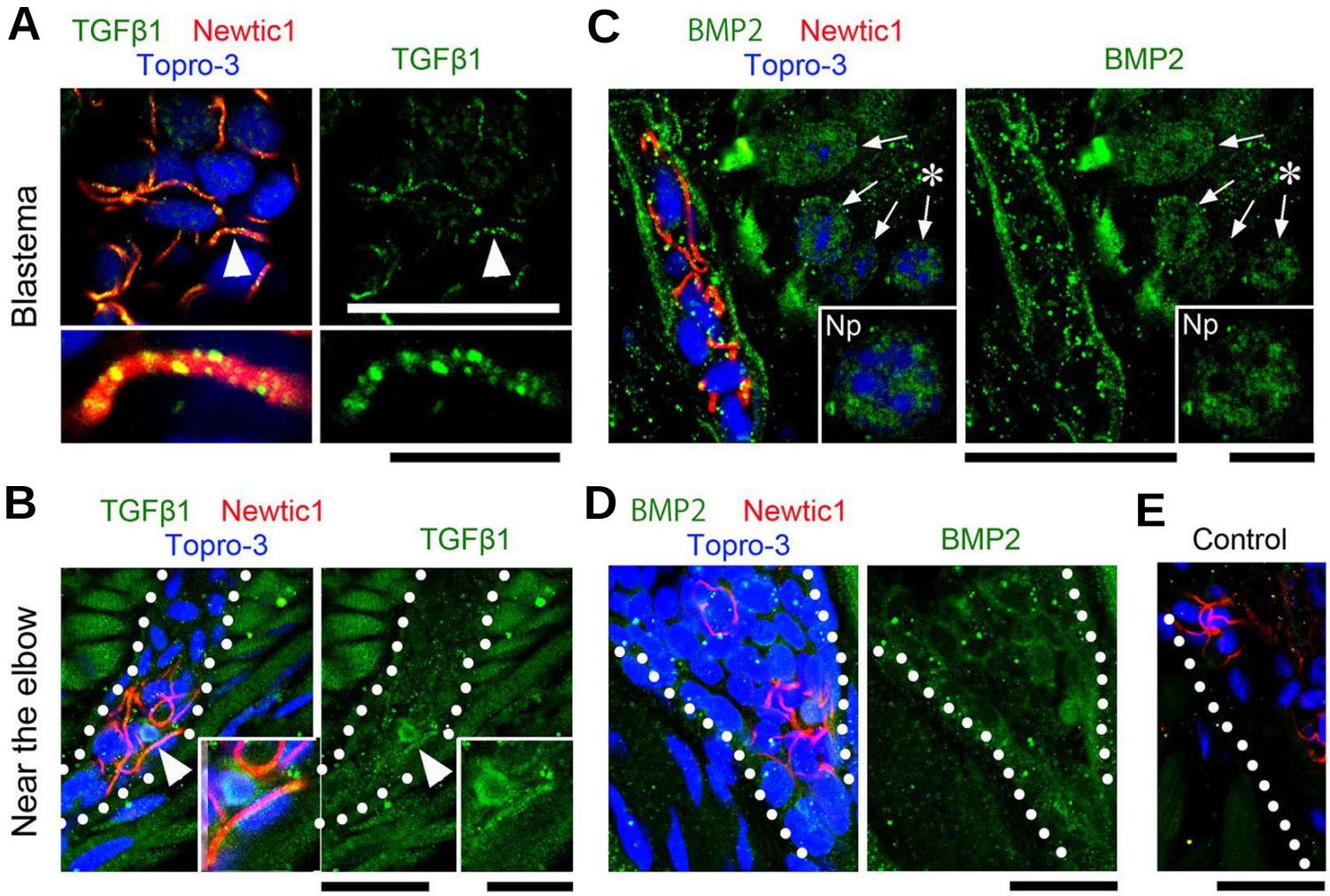
A
TGFβ1 Newtic1
Topro-3
TGFβ1
Blastema
C
BMP2 Newtic1
Topro-3
BMP2
Np
Np
B
TGFβ1 Newtic1
Topro-3
TGFβ1
Near the elbow
D
BMP2 Newtic1
Topro-3
BMP2
E
Control

Fig 21. EryCs deliver TGFβ-1 and BMP2 into the growing blastema.

(A) Representative image showing TGFβ-1 expression in EryCs in a growing blastema (n = 3). The section was obtained from a regenerating limb in a transitional stage from stage II to stage III. Intense TGFβ-1 immunoreactivity was observed in a large number of dots located along the equatorial plane of most PcNobs, though the cytoplasm of PcNobs exhibited weak immunoreactivity. A sample indicated by the arrowhead was enlarged in the lower panel. Topro-3: nucleus. Scale bars, 50 μm (upper) and 10 μm (lower). **(B)** Representative image showing TGFβ-1 expression in PcNobs circulating along the thick blood vessels near the elbow (n = 3). The section was obtained from the same limb in (A). Dotted lines show the vessel wall. TGFβ-1 immunoreactivity in PcNobs was substantially the same as that observed in blood cell suspensions, though it was difficult to recognize differences in immunoreactivity between EryCs and free Newtic1-negative PcNobs. Inset: enlarged image of the equatorial plane of PcNob (arrowhead). Scale bars, 50 μm and 10 μm (inset). **(C)** Representative image showing BMP2 expression in EryCs in a growing blastema (n = 3). The section was obtained from a regenerating limb in the transitional stage from stage II to stage III. BMP2 immunoreactivity in the cytoplasm of PcNobs obviously declined while intense immunoreactivity was observed in small dots distributed around the PcNobs as well as along the wall of regenerating capillaries/vessels. Arrows: neutrophil (Np) which exhibited BMP2 immunoreactivity in its cytoplasm. Inset: enlargement of the neutrophil (asterisk). Scale bars, 50 μm and 20 μm (inset). **(D)** Representative image showing BMP2 expression in PcNobs circulating along thick blood vessels near the elbow (n = 3). The section was obtained from the same limb in (C). Dotted lines show the wall of the vessel. BMP2 immunoreactivity in PcNobs was substantially the same as that observed in blood cell suspensions. Scale bars, 50 μm. **(E)** Example showing control immunoreactivity with Newtic1 (red) and RFP (green) antibodies (n = 3). The image shows tissues near the elbow. Dotted lines show the vessel wall. The section was obtained from the same limb in (C,D). Scale bars, 50 μm (image adapted from Casco et. al, 2018).

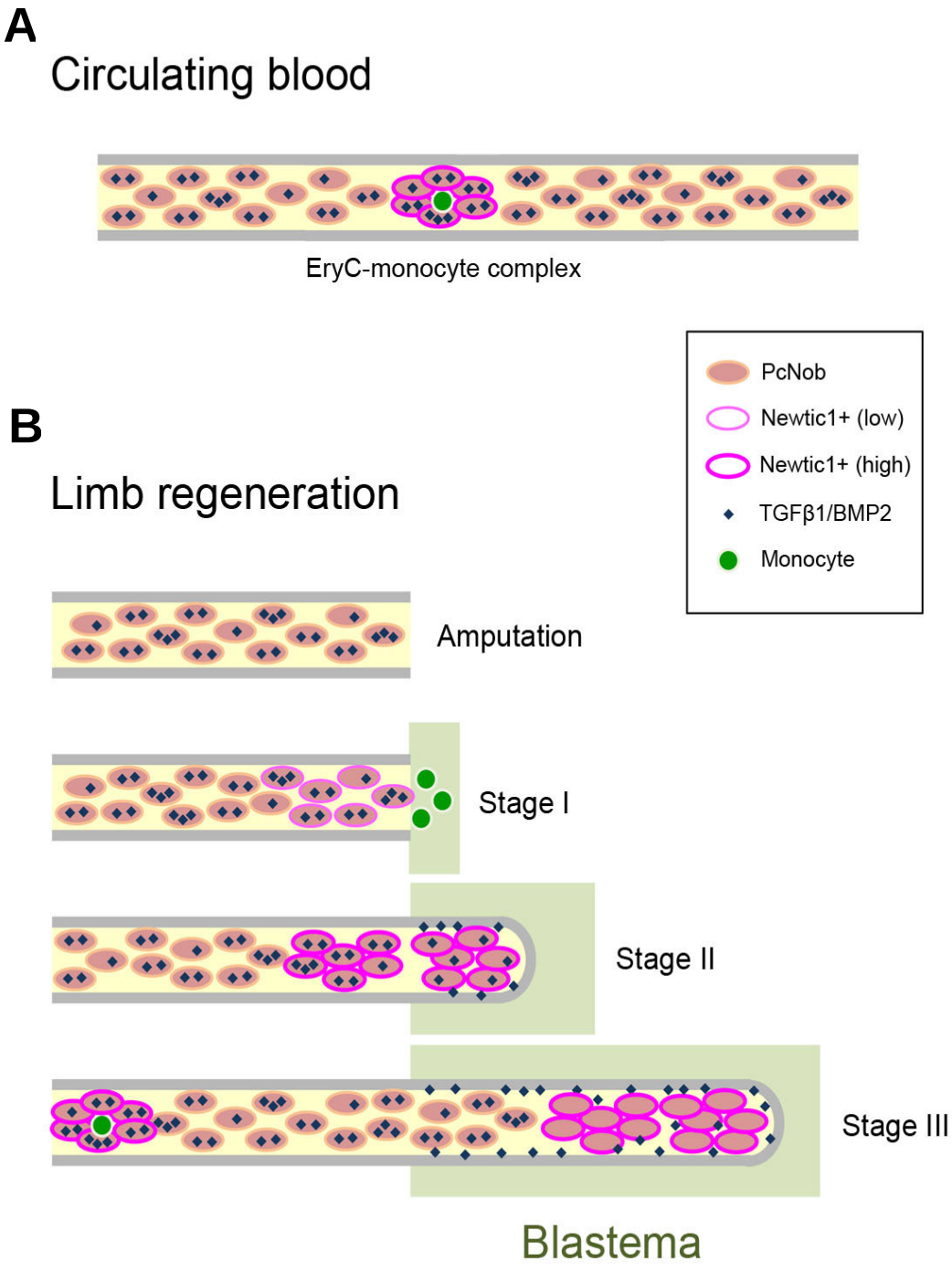
A
Circulating blood
EryC-monocyte complex
B
Limb regeneration
PcNob
Newtic1+ (low)
Newtic1+ (high)
TGFβ1/BMP2
Monocyte
Amputation
Stage I
Stage II
Stage III
Blastema

Fig. 22 Summary

(A) Circulating blood. Newtic1+ PcNobs form EryC-monocyte complexes, and circulate together with free Newtic1- PcNobs. PcNobs and EryCs carry secretory molecules such as TGFβ-1 and BMP2. **(B)** Limb regeneration. After the wound closes, PcNobs near the amputation site start to express Newtic1 (stage I). Newtic1+ PcNobs form EryCs. EryCs are translocated into the growing blastema as the capillaries/vessels regenerate (stage II). EryCs accumulate in the distal part of the growing blastema as angiogenesis proceeds (stage III). PcNobs in EryCs seem to release TGFβ-1 and BMP2, both of which are then attached to the surface (along the equatorial plane) of PcNobs or matrices along the endothelium of capillaries/vessels (image adapted from Casco et. al, 2018).

10. TABLES

Table 1. *IS*-transcripts in the transcriptome of limb blastema (Stage I-III), In which 9 correspond to the genes that have been suggested to be involved in limb regeneration (table adapted from Casco et. al, 2018).

IS-transcript	Gene	Blast description	References
comp197402_c0_seq1	RARb	Retinoic acid receptor beta isoform x4	Giguere et al. 1989, Ragsdale et al. 1989, Carter et al, 2011. Nguyen et al. 2017
comp44533_c0_seq3	LHX2	LIM/homeobox protein Lhx2 isoform X2	Showalter et al. 2004, Shimokawa et al. 2014.
comp44198_c0_seq2	SALL1	Sal-like protein 1 isoform x1	Neff et all 2011, Knapp et al. 2013, Stewart et al. 2013
comp34287_c0_seq2	ZFHX4	Zinc finger homeobox 4	Monoghan et al 2012
comp46610_c1_seq1	MSX1	Msx1 protein	Carlson et al. 2012, Koshiba et al, 1998, Kumar et al. 2004
comp37101_c0_seq1	TWT2	Twist-related protein 2	Satoh et al. 2008
comp25086_c0_seq1	CRABP1	Cellular retinoic acid-binding protein 1	Monoghan et al. 2012, McEwan et al. 2011, Kochegarov et al. 2015, McCuster e tal 2015.
comp122669_c0_seq1	SHH	Sonic Hedgehog	Imokawa et al 1998, Torok et al. 1999, Nacu et al 2016. Hubbard et al. 2002.
comp46084_c0_seq1	SCXB	Basic helix-loop-helix transcription factor scleraxis	Satoh et al. 2006
comp25123_c0_seq1	FGF10	Fibroblast growth factor 10	Christensen et al. 2001, Han et al 2001, Christsen et al 2002, Knapp et al. 2013,
comp3297_c0_seq1	FRZ7	Frizzled-7	Girich et al, 2017
comp27330_c0_seq1	WNT9A	Wingless-type MMTV integration site family member 9a	Kawakami et al. 2006, Spater et al. 2006, yokoyama et al. 2007

Table 2. PCR primer sets and amplicon size (table adapted from Casco et. al, 2018).

gene	Primer Sequences		Amplicon Size (bp)	Cycle number
	Forward	Reverse		
RARb	TCCCAAAGTCCGAGGTCAAG	AGAAGGAGCCGATAAAACAGGA	181	40
LHX2	TTCAAACACCACCAGTTGCG	CTCCTGTGTTTTCTTGGCGT	188	40
WNT 9A	GCATTCCACATAGCAGCACC	GGACTACAGACCTGACCTAT	200	40
SALL 1	TTGCTTGTCAGAGTGCCTTG	TGCTGCTTCAAATTACCCTTT	112	40
ZFHX4	GGCTTTCCCAAATACCTCAGC	GGAACATCTTTGGACACACAGG	144	40
MSX1	TCTCTACATGGCTTCTGTCCA	CTTGTCCGGCTCCTCGTC	112	40
TWIST2	ATCATCCCCACACTGCCCT	GCTTGAGGGTCTGGATCTTAC	52	40
CRABP1	TGCACACAACATCATCAGC	GAGATCAACTTCAAAATCGGGGA	209	40
SHH	GGCTTCGACTGGGTCTACTT	AATCCTCACCCCTTGCTCC	135	40
SCXB	GCACCAACAGCGTCAACA	GGTGGGAGATGTAGCTGGAG	181	40
FGF10	ATGTTTCTTCTTGTGAGGCGT	CACCCTTCCTCAGTACCCAT	112	40
FRZD1	GCCATGCCGAAGAAGTAGA	AGCGGCCCATCATCTTCCT	190	40
EF1a	GACCTTTGCCCCCAGTAACGTAACCAC	ACTGGGTGTTGCTGGCGCTACTTCTTG	573	25
NEWTIC1 LONG	CTTGTGAGGATTACATTGTGCA	GCTCGTGTGAAACCTAAGAGA	1,512	35
NEWTIC1 Short	GGTTGGTCGAAAAGAGTCAGA	GCCCTATGCATGAAAGTTGG	76	30
NEWTIC1 Semi Q. Anal.	TTTCCCACCATGCACCTCCTCGTA	CCTTCCTGTGGGCTCTGATGTCCA	497	35
TGFβ1	GTAGTTGTGGACAGACATTGGGCGTGT	TTGTAAAGCACCATGACTTCCTCGGGC	433	30
BMP2	AGAATAACAAGGCACCAGAACACGCCA	ATCCCGGCCACCATTGTCAACCTAAAG	511	30
VEGFC	GTGATTATGCCCCATTCCTGCTCTGCT	CACACCGGTTCCTTCTGTTGTATCCCC	650	30
PDGFC	CGATGAGTATATCCCCTCCGCTCCTGG	GCCGTCTAGCCTTCTGTATTCCCTTTGC	606	30
IGF II	GTTCATTTCCGCCTGTCCGATGTCTCT	GCTCTGAAGGTGCCCAAGATGACTGTG	584	30
nsCCN	GACTGCAATGACCTACGACCCTGTGAC	TCTTCCCACCCTTGATGACCGTGTACT	658	25
COL-a	GAATGAGAGAGACCGAGAGAGTGACCA	CAGAAAAGCTCCGTGAAATGCAGCAAT	505	35
COL-b	AAGCTGATGGAGTGGTAGGCCCTGTAG	TTTGGATTGGAGGTCACTGGGAAGCTG	628	35
MMP21	GGTAATCGCCCAGTTCTCCATTCGCTT	ATCAACCAGAACTCACCCTCAGTCCCA	957	35
MMP9	CTCACCTTCACTCAGATCTACAGCGGC	TTGGGTCTTCACGTCCAACCTCCAGTA	1,389	30

Table 3. Sequences corresponding to Newtic1 in other vertebrates (Blast results with E: <e-5). ND indicates no difference (table adapted from Casco et. al, 2018).

Species	Genome database[59]				
	Genome	cDNAs	cDNAs *ab initio*	Peptide	Peptide *ab initio*
Human (*Homo sapiens*)	ND	ND	ND	ND	ND
Opossum (*Monodelphis domestica*)	ND	ND	ND	ND	ND
Chicken (*Gallus gallus*)	ND	ND	ND	ND	ND
Anole lizard (*Anolis carolinensis*)	ND	ND	ND	ND	ND
Frog (*Xenopus tropicalis*)	ND	ND	ND	ND	ND
Coelacanth (*Latimeria chalumnae*)	ND	ND	ND	ND	ND
Zebrafish (*Danio rerio*)	ND	ND	ND	ND	ND
	Transcriptome database				
Axolotl (*Ambystoma mexicanum*)	Hit (ID: AMEXTC_0340000020965)				
Red spotted newt (*Notophthalmus viridescens*)	Hit (ID: com1037174_c0_seq1)				
Iberian ribbed newt (*Pleurodeles waltl*)	Hit (Reconstructed in this study)				

Antibody	Dilution	Provider
Primary		
Rabbit anti-Newtic1 polyclonal antibody	1:200	Custom made; Merck (Sigma-Aldrich), Tokyo, Japan
Rabbit anti-RFP polyclonal antibody	1:500	600-401-379; Rockland Immunochemicals, PA 19468, USA
Rabbit anti-TGFb1 polyclonal antibody	1:500	CYT4632; Celltechgen LLC, TX 77079, USA
Rabbit anti-BMP2 polyclonal antibody	1:500	LS-B13128; LifeSpan BioSciences, InC., WA 98121, USA
Mouse anti-vimentin monoclonal antibody	1:500	ab28028; Abcam,Tokyo, Japan
Secondary		
Alexa Fluor 488-conjugated goat anti-mouse IgG (H + L) polyclonal antibody	1:500	A11001; Thermo Fisher Scientific, Tokyo, Japan
Rhodamine (TRITC)-conjugated affiniPure goat anti-rabbit polyconal antibody	1:500	111-025-003; Jackson ImmunoResearch Laboratories, PA 19390, USA
Biotinylated goat anti-rabbit IgG polyclonal antibody	1:500	BA-1000; Vector laboratories, CA 94010, USA

Table 4. Antibodies for immunolabeling (table adapted from Casco et. al, 2018).